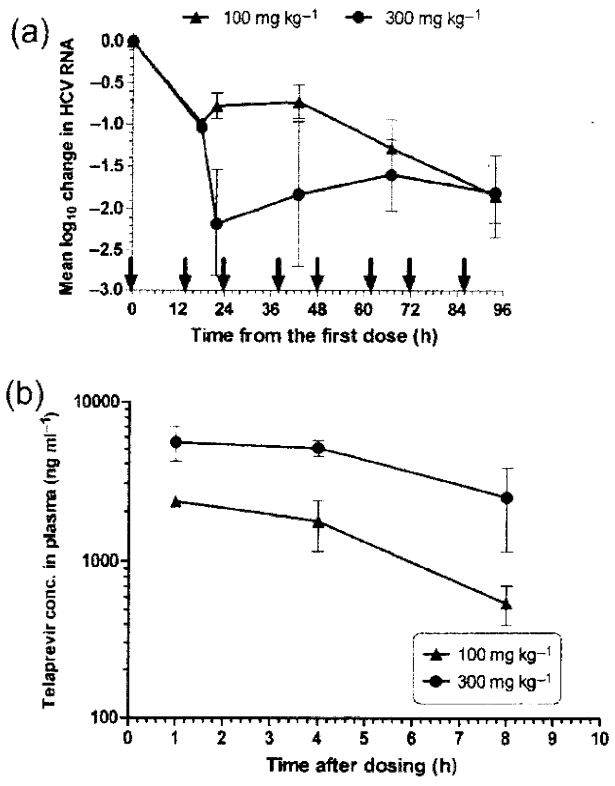

Fig. 3. PK analysis of telaprevir in the HCV-infected mouse model. Six HCV-infected mice were administered 100 (n=3) or 300 (n=3) mg telaprevir kg^{-1} BID for 4 days and serum samples were collected once daily to assess antiviral activity. After the last dose, plasma samples were collected at 1, 4 and 8 h for PK analysis. (a) Mean $\log_{10}$ changes (± SEM) in serum HCV RNA from mice treated with telaprevir. Arrows indicate the times of dosing. (b) Kinetics of telaprevir concentrations in plasma after the last dose.

10-fold higher at 5 h and approximately fourfold higher at 8 h than those in plasma. Total cellular RNA samples were extracted from two, one and four discrete small sections (approx. 50 mg) of the liver in the preliminary dose-finding, PK and PK/PD cohorts, respectively. HCV RNA levels in the total cellular RNA extract were relatively quantified by duplex real-time RT-PCR analysis using human β_2-microglobulin (hβ_2m) as an internal standard of human endogenous gene expression. Neither the threshold cycle (Ct) of hβ_2m ($Ct_{h\beta 2m}$) nor the Ct of HCV (Ct_{HCV}) correlated with total RNA from a small section of the chimeric human livers (data not shown). This result indicated that occupancy rates of human cells varied individually and/or among small sections of the chimeric human liver. Therefore, the mean difference in Ct ($\Delta Ct = Ct_{HCV} - Ct_{h\beta 2m}$) in each mouse was calculated and plotted against the viral load in serum (Fig. 6). After treatment with telaprevir for up to 10 days, mean ΔCt values ranged between 11 (HCV RNA content: $2^{11} = 2 \times 10^3$-fold lower than hβ_2m expression) and 17 (1×10^5-fold lower) among the HCV-infected mice and correlated linearly with $\log_{10}$ serum HCV RNA levels.

Viral dynamics model analysis

To evaluate time-dependent reductions in HCV with BID dosing, 12 HCV-infected elderly mice, which maintained high and steady-state viral loads (1.2×10^6–8.5×10^7 copies ml^{-1}) for more than 6 months, were treated with 200 mg telaprevir kg^{-1} BID for 3 days. The mice were divided into two groups, and serum samples were collected just before the second dose and 4 (n=6) or 8 (n=6) h after every two administrations. The single administration of telaprevir resulted in a mean 0.8–1.0 $\log_{10}$-fold reduction in HCV RNA in both groups. After the second dose, the pattern of viral kinetics appeared to depend on the time of serum collection, and the mean HCV RNA reduction level was higher in the 8 h group than in the 4 h group and plateaued at approximately a 2 $\log_{10}$-fold reduction in both groups after treatment for 3 days (Fig. 7). Finally, we attempted to estimate parameters of efficacy (ε) and virus clearance (c) per hour in this mouse model for comparison with estimates derived from human studies. Because the mean viral kinetics of the 8 h group was biphasic, the values in the 8 h group were used together for the mathematical model analysis. The estimated ε and c values were 0.992 (95 % CI 0.982–1.00) and 0.200 (95 % CI 0.110–0.291), respectively.

DISCUSSION

Using a mouse model with a chimeric human liver for HCV infection, we analysed the PK/PD of telaprevir treatment and investigated HCV dynamics during the initial phase of protease inhibitor treatment. All the mice in this study were expected to have more than half of their livers repopulated by human hepatocytes (Tateno *et al.*, 2004), which simulates a human drug metabolism profile (Katoh *et al.*, 2007, 2008). After the infection with HCV genotype 1b, high viral loads were maintained in the mice for more than 6 months. Recent studies have indicated the utility of a human/mouse chimera model for HCV infection to evaluate antiviral efficacy (Kneteman *et al.*, 2006, 2009) and preclinical safety (Vanwolleghem *et al.*, 2007). However, PK/PD studies and estimations of virus clearance rate have rarely been performed in this mouse model. HCV production, including intracellular replication in engrafted hepatocytes, has also not yet been elucidated. Despite the SCID nature of this mouse model, a 2 $\log_{10}$-fold HCV RNA reduction was observed within 0.5 days, as has been observed previously in CHC patients (Forestier *et al.*, 2007; Reesink *et al.*, 2006). In this mouse model, the rapid rebound in HCV load during the intermission from drug exposure indicated the rapid production and release of HCV into the circulation. This finding indicates that a virion-clearing compartment, which does not depend on T- and B-cell responses, may exist in this mouse model.

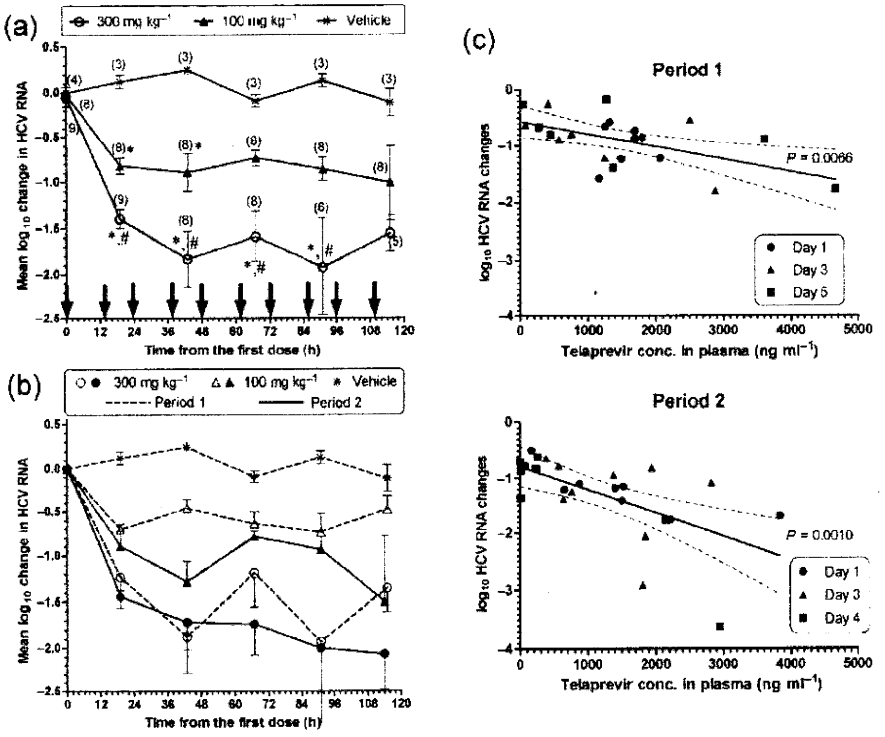

Fig. 4. PK/PD analysis and the dose-dependent reduction in HCV. Twelve HCV-infected mice were randomized into three groups (n=4 each) and then underwent two periods of telaprevir BID dosing for 5 days, separated by a 1-week washout period. Before the second period, the mice in the vehicle control group were additionally assigned to active drug groups. During the second period, mice that received the high or low doses were crossed over to the alternative treatment. Serum and plasma samples were collected once daily 5 h after dosing. Mean $\log_{10}$ changes (± SEM) in serum HCV RNA were calculated from the combined results from both periods (a) and each period separately (b). Arrows indicate the times of dosing. *, $P<0.05$ versus vehicle control group; #, $P<0.05$ versus 100 mg kg^{-1} group. (c) Correlation between $\log_{10}$ reduction in serum HCV and telaprevir concentrations in plasma. Linear regressions (solid lines) and 95 % CI (dashed lines) are indicated.

One possible explanation is that viral kinetics after liver transplantation in humans may play a role in HCV clearance under immunosuppressed conditions (Dahari *et al.*, 2005; Powers *et al.*, 2006; Schiano *et al.*, 2005). This observation suggests that this mouse model is capable of evaluating 'first-phase' HCV clearance after drug treatment.

In a clinical trial of telaprevir, CHC patients who exhibited a continuous decline in viral kinetics had mean plasma trough levels above 1000 ng ml^{-1}; therefore, a dose of 750 mg TID was selected for further clinical studies (Sarrazin *et al.*, 2007). When HCV-infected mice were administered 100 or 300 mg telaprevir kg^{-1}, a plasma concentration above 1000 ng ml^{-1} was maintained beyond 8 h in mice treated with 300 mg kg^{-1} but not in those treated with 100 mg kg^{-1}. This result suggests that the extrapolation of telaprevir doses from this mouse model to human studies depends on body surface area, i.e. approximately 15th of a dose in this mouse model may be equivalent to a dose in humans. In another cohort of mice treated with 100 and 300 mg telaprevir kg^{-1} BID, a dose-dependent reduction in HCV was observed and the plasma telaprevir concentration correlated significantly with the HCV reduction level. Therefore, the PK/PD results in this mouse model may be able to indicate a targeted dose range in clinical studies.

Whereas a telaprevir concentration in plasma equivalent to its dosage in clinical trials was achieved in this mouse model, the serum HCV RNA level plateaued at a decrease of approximately 2 $\log_{10}$-fold within several days of treatment. A saturated reduction of approximately 2 $\log_{10}$-fold after treatments with BILN 2061 and IFN was also reported in an analogous mouse model (Kneteman *et al.*, 2006; Vanwolleghem *et al.*, 2007). These observations led us to examine HCV replication in the chimeric human liver. In the relative quantification of HCV RNA against human-specific endogenous gene expression, we observed a correlation between the serum HCV RNA level and the mean ΔCt value in the liver, despite no correlation between the total RNA concentration and each Ct value of two target genes in the liver RNA extracts. This result can be interpreted to indicate that HCV replicated only in

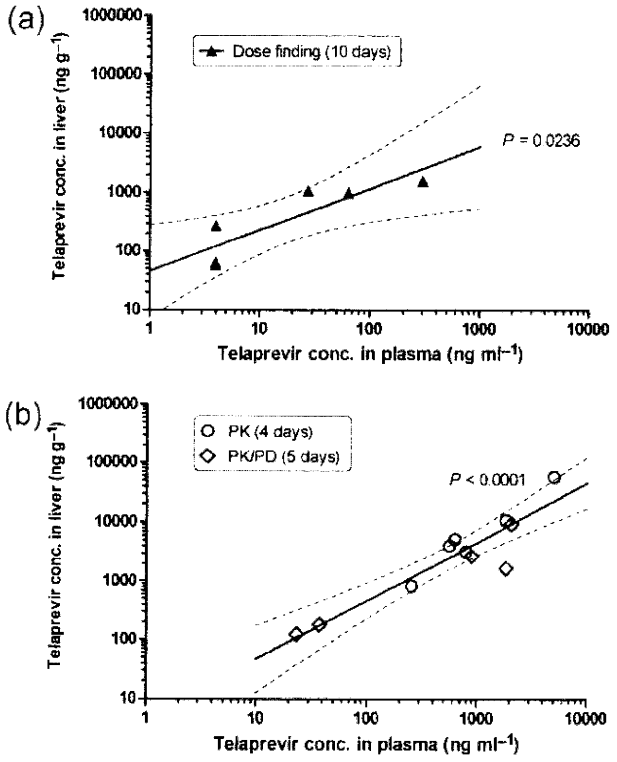

Fig. 5. Correlation between telaprevir concentrations in the liver and plasma. Telaprevir concentrations in the liver and plasma were determined at the end of the three different experiments indicated in Fig. 1 (dose-finding), Fig. 3 (PK) and Fig. 4 (PK/PD). Telaprevir concentrations in the liver were plotted against those in plasma 5 (a) or 8 (b) h after the last dose. Linear regressions (solid lines) and 95 % CI (dashed lines) are indicated.

engrafted human hepatocytes, and the observed HCV reduction in serum might reflect virus replication in the human hepatocyte grafts. Moreover, the relative content of HCV RNA was 2×10^3–1×10^5-fold lower than hβ_2m expression, whereas an HCV replicon cell line, which had approximately 1000 replicon genomes per cell (Quinkert *et al.*, 2005), contained nearly equal amounts of both genes (data not shown). HCV replication was much lower in the engrafted human hepatocytes than in an HCV replicon cell line, and HCV infected only a small portion of the engrafted human hepatocytes. It has been reported that 4–25 % of hepatocytes in a CHC patient were positive for replicative-intermediate RNA, and the mean number of viral genomes per productively infected hepatocyte ranged from 7 to 64 molecules (Chang *et al.*, 2003). Also, a more recent report suggested that the percentage of HCV antigen-positive hepatocytes in patients varied from 0 to 40 %, and the HCV content in 2000 microdissected HCV-positive cells ranged from 40 to 1800 international units using a branched DNA assay (Vona *et al.*, 2004). Therefore, we suggest that HCV replication efficiency in engrafted human hepatocytes is equivalent to that in CHC patients.

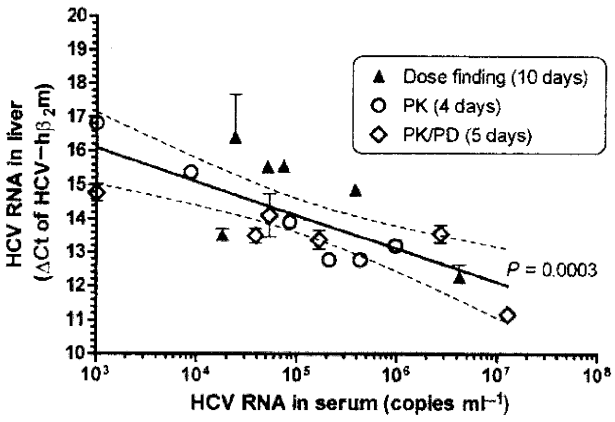

Fig. 6. Correlation between HCV content in the liver and serum. Relative quantification of HCV RNA levels in the liver was determined by the difference between threshold cycles (ΔCt) of HCV RNA and hβ_2m in a duplex real-time RT-PCR analysis. Linear regressions (solid line) and 95 % CI (dashed lines) are indicated.

The differences observed between the engrafted human hepatocytes and the HCV replicon cell line can be explained by the following assumptions: approximately 10 % of engrafted human hepatocytes are productively

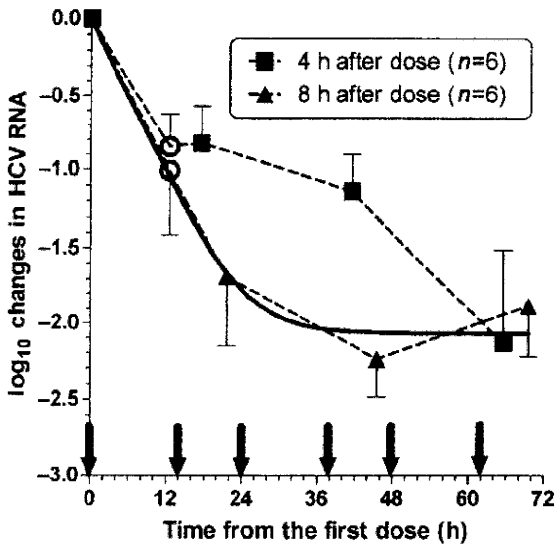

Fig. 7. Viral dynamics under BID telaprevir treatment. Mice were administered 200 mg telaprevir kg^{-1} BID at the times indicated by arrows. Serum samples were collected just before the second dose was administered and 4 (n=6) or 8 (n=6) h after every two doses were administered. Mean $\log_{10}$ changes (± SEM) in serum HCV RNA are plotted. The solved equation described in Methods was fitted to the values in the 8 h group (solid line), and the estimated efficacy and virion clearance rates were 0.992 (95 % CI 0.982–1.00) and 0.200 (95 % CI 0.110–0.291), respectively.

infected and harbour approximately ten HCV genomes per cell at baseline steady state and a 2 $\log_{10}$-fold reduction is achieved with drug treatment.

Mathematical models have proven valuable in understanding the *in vivo* dynamics of HCV, and very rapid dynamic processes occur on timescales of hours to days, and slower processes occur on timescales of weeks to months (Perelson & Ribeiro, 2008). In the last experiment, we observed a biphasic decline in the HCV RNA level after BID dosing for 3 days. During the first 2 days of the treatment, a discrepancy in viral kinetics between the serum-sampling time points was noted. Similarly, fluctuations in viral kinetics during the first-phase slope were observed in patients who received IFN three times a week (Pawlotsky *et al.*, 2004). Variable efficacy rate determined by PK parameters can explain fluctuations during the first-phase slope in mathematical model analysis (Talal *et al.*, 2006). However, it is difficult to evaluate the individual temporal changes in viral and drug kinetics using a mouse model as only a limited volume of blood is available for analysis. Therefore, we assumed a constant efficacy rate (ε) and omitted a turnover rate of hepatocytes because of the short duration of treatment. The estimated clearance rate (c) in this study was 4.8 day^{-1}. Additionally, the mean slope of 0.144 $\log_{10}$ h^{-1} (Fig. 2b) could be transformed to 0.332 h^{-1}=8.0 day^{-1} according to the change of base of a logarithm. The estimated clearance rates in this mouse model basically agreed with estimates determined in humans infected with HCV genotype 1 and undergoing IFN-based therapies (Herrmann *et al.*, 2003; Neumann *et al.*, 1998; Pawlotsky *et al.*, 2004) or large-volume plasma apheresis (Ramratnam *et al.*, 1999). Total virion production during steady-state viral kinetics in this mouse model was calculated by multiplying c by the initial viral load (V_0) and then normalizing the extracellular fluid volume. From previous studies, it was determined that 10^{11}–10^{13} virions are produced daily in patients with high HCV loads (Neumann *et al.*, 1998; Ramratnam *et al.*, 1999). In this mouse model, the volume of extracellular fluid and weight of the liver were approximately 20 and 9% of the body weight (data not shown), and the mean $\log_{10}$ V_0 ($\pm$SEM) among the mice with mean clearance rates of 4.8 and 8.0 per day were 6.96$\pm$0.26 and 7.00$\pm$0.33, respectively. The results of the calculations indicated that 1 g of the chimeric human liver produced 1×10^8–2×10^8 virions per day. The typical weight of the human liver is 1–2 kg; thus, the capacity of human hepatocytes to produce HCV in this mouse model may be equivalent to that in CHC patients. In conclusion, a mouse model with a chimeric human liver can simulate HCV replication in human patients quantitatively and dynamically, and this mouse model may be suitable for preclinical evaluations of novel HCV-specific agents and other therapeutic strategies, including combination regimens.

METHODS

Generation of mice with chimeric human livers and HCV infection. The generation of $uPA^{+/+}/SCID^{+/+}$ mice and transplantation of frozen human hepatocytes was performed at PhoenixBio. Graft function was monitored on the basis of HSA levels in blood (Tsuge *et al.*, 2005). All the mice had high HSA levels, which suggested that nearly half of their livers were repopulated by human hepatocytes (Tateno *et al.*, 2004). After obtaining written informed consent, we collected sera periodically from patients who were chronically infected with HCV genotype 1b and failed to respond to PEG-IFN and RBV therapy. The mice were inoculated with the serum samples via the orbital vein after anaesthetization. The experimental protocol was approved by the Ethics Review Committee for Animal Experimentation of the Graduate School of Biomedical Sciences, Hiroshima University.

Compound preparation and experimental designs. The telaprevir formulations were kindly provided by Vertex Pharmaceuticals. A telaprevir suspension was prepared as described previously (Perni *et al.*, 2006) and used in experiments 1 and 2. In the other experiments, a telaprevir suspension was prepared daily as in the tablet formulation (Forestier *et al.*, 2007; Hézode *et al.*, 2009; McHutchison *et al.*, 2009). A suspension of telaprevir was administered via oral gavage.

Experiment 1: preliminary dose-finding study. Ten out of 11 mice developed serum HCV loads greater than 10^4 copies ml^{-1}. Nine mice with high viral loads ($>10^5$ copies ml^{-1}) were randomized and administered 10 or 100 mg telaprevir kg^{-1} BID or TID over three periods. During period 1, the mice were administered 100 (n=4) or 10 (n=4) mg telaprevir kg^{-1} or vehicle (n=1) BID at 18:00 and 10:00 h for 7 days, and serum samples were collected before treatment and 1 h after administration in the morning on the third and/or seventh day. During period 2, the mice were administered 100 (n=5) or 10 (n=4) mg telaprevir kg^{-1} TID for 3 days, and serum samples were collected before treatment and 4 h after administration of the last dose. Three mice died between periods 2 and 3. During period 3, the mice were administered 100 (n=3) or 10 (n=3) mg telaprevir kg^{-1} TID for 10 days. The mice were sacrificed 5 h after administration of the last dose, and plasma, serum and liver samples were collected.

Experiment 2: evaluation of HCV turnover. Eleven mice were infected with HCV and eight mice survived for more than 15 weeks with steady-state and high viral loads (10^6–10^8 copies ml^{-1}). Six of the mice were administered 200 mg telaprevir kg^{-1} TID at 9:00, 14:00 and 19:00 h for 4 days. On day 1, serum samples were collected before dose administration, 4 h after the first and second doses were administered, and 2 h after the third dose was administered (n=2 each). On day 2, serum samples were collected 1 h after each of the three doses was administered (n=2 each). Serum samples were also collected 4 h after the first and second doses were administered on day 3 (n=3 each) and 4 h after the second dose was administered on day 4.

Experiment 3: PK analysis. After a washout period, six mice from experiment 2 were administered 100 or 300 mg telaprevir kg^{-1} (n=3 each) BID at 19:00 and 9:00 h for 4 days. Serum samples were collected before dose administration, 4 (n=1) or 8 (n=2) h after administration of the second dose, and 5 h after every two doses were administered. After the final dose was administered, plasma for PK analysis was collected at 1 and 4 h. The mice were sacrificed at 8 h, and serum, plasma and liver samples were collected.

Experiment 4: dose dependence and PK/PD analysis. Thirty-six mice were infected with HCV and 13 survived for more than 13 weeks. The median survival time of this cohort was 81 days after infection. Twelve HCV-infected mice were randomized into three groups (A–C; n=4 each) and underwent two periods of BID dosing for 5 days, which were separated by 1-week washout periods. During the first period, the mice in groups A, B and C were administered 300 mg telaprevir kg^{-1}, 100 mg telaprevir kg^{-1} and vehicle,

respectively. Because two mice in group A and two mice in group C died before the second period, two remaining mice in group C and one back-up mouse were assigned to group A (n=2) and group B (n=1). During the second period, mice that received high or low doses were crossed over to the alternative treatment. Serum samples were collected before the first dose was administered and 5 h after every two doses were administered. Plasma samples were also collected at the same time on days 1, 3 and 5 in the first period and days 1, 3 and 4 in the second period. The mice were sacrificed 8 h after administration of the final dose, and serum, plasma and liver samples were collected.

Experiment 5: viral kinetics with BID dosing After infection of 45 mice, 12 HCV-infected mice maintained steady-state and high viral loads (1.2×10^6–8.5×10^7 copies ml^{-1}) for more than 6 months. The median survival time of this cohort was 131 days after infection. These mice were treated with 200 mg telaprevir kg^{-1} BID at 19:00 and 9:00 h for 3 days. The mice were divided into two groups and serum samples were collected just before the second dose was administered and 4 (n=6) or 8 (n=6) h after every two doses were administered.

Serum RNA extraction and HCV RNA quantification. HCV RNA was isolated from 10 µl serum under denaturing conditions using a SepaGene RV-R kit (Sanko Junyaku). The dried precipitates were dissolved in 10 µl diethylpyrocarbonate-treated water. Extracts were duplicated and assayed by quantitative real-time RT-PCR using TaqMan EZ RT-PCR core reagents (Applied Biosystems). Nucleotide positions of the probe and primer sets refer to HCV H77 strain (GenBank accession no. AF009606). The TaqMan probe 5′-6-FAM-CTGCGGAACCGGTGAGTACAC-BHQ-1-3′ (nt 148–168) was purchased from Biosearch Technologies, and the forward (5′-CGGGAGAGCCATAGTGG-3′; nt 130–146) and reverse (5′-AGTACCACAAGGCCTTTCG-3′; nt 272–290) primers were purchased from Sigma-Aldrich. The 25 µl RT-PCR mixture contained 0.2 nmol forward and reverse primers ml^{-1}, 0.3 nmol TaqMan probe ml^{-1} and 5 µl extracted RNA, and was monitored using a PRISM 7900HT sequence detection system (Applied Biosystems). The thermal profile was 2 min at 50 °C, 30 min at 60 °C for reverse transcription and 5 min at 95 °C, followed by 45 cycles of 20 s at 95 °C and 1 min at 62 °C. The HCV replicon I_{389}neo/NS3-3′/5.1 (Lohmann *et al.*, 1999) RNA was transcribed *in vitro* using a T7 RiboMax Express Large Scale RNA Production System (Promega) and purified twice using gel filtration. The concentration of this transcribed RNA was determined by absorbance at 260 nm and serially diluted 10-fold to prepare a standard curve for each assay.

Liver RNA extraction and HCV RNA quantification. A Wizard SV total RNA Isolation System (Promega) was used to obtain a DNase I-treated total RNA sample. The total RNA concentration was determined by absorbance at 260 nm. Total RNA samples were assayed by duplex real-time RT-PCR for relative quantification of HCV RNA using endogenous control gene expression of human β_2-microglobulin (hβ_2m; GenBank accession no. NM_004048), the TaqMan probe 5′-CAL Fluor Orange 560-AGTGGGATCG-AGACATGTAAGCAGCATCAT-BHQ-1-3′ (nt 401–430), and the forward and reverse primer set of 5′-TTGTCACAGCCCAA-GATAGTT-3′ (nt 379–399) and 5′-TGCGGCATCTTCAAACC-3′ (nt 434–450). To adjust the efficacy of PCR amplification of both target genes, the reaction condition was modified from the HCV single-probe assay. The temperature for extension was 60 °C, the concentration of the HCV probe was 0.24 nmol ml^{-1} and the reaction mixture contained the TaqMan probe/primer set for hβ_2m: 0.2 nmol primers ml^{-1} and 0.12 nmol TaqMan probe ml^{-1}. Because both target genes double after one cycle of PCR, a difference in Ct between HCV and hβ2m ($\Delta Ct = Ct_{HCV} - Ct_{h\beta2m}$) theoretically indicates a relative quantity of HCV RNA per control gene expression of $2^{-\Delta\Delta Ct}$.

Determination of drug concentration. Plasma and liver samples were analysed using chiral liquid chromatography followed by tandem mass spectrometry. After reconstitution, sample extracts were separated by normal-phase chromatography on a 2 × 250 mm Hypersil CPS-1 column (Thermo Hypersil-Keystone) with a mobile phase of heptane : acetone : methanol (82 : 17 : 1). Analyte concentrations were determined by turbo ion spray liquid chromatography/tandem mass spectrometry in the positive-ion mode. Analysis was performed at SRL or Mitsubishi Chemical Medience.

Statistical analysis. The HCV RNA level in serum was normalized by logarithmic conversion. Statistical analysis was performed with a mixed linear model using SAS (SAS Institute). Mean differences between two groups were evaluated with Student's t-test. The difference compared with vehicle control at each time point was evaluated by Dunnett's multiple comparisons test. Linear and non-linear regression analyses were performed using GraphPad Prism 5 (GraphPad Software).

Viral dynamics model analysis. The basic mathematical model for the analysis of HCV infection *in vivo*, which is a system of three ordinary differential equations for uninfected cells (T), productively infected cells (I) and free virus (V), has been reviewed elsewhere (Perelson & Ribeiro, 2008). Briefly, one of the three equations ($dV/dt = pI - cV$), where viral particles are produced at rate p per infected cell and cleared at rate c per virion, was solved. During treatment for 2–3 days, if one assumes that the number of I is approximately constant and equal to its pre-treatment value and that the viral level was at its set-point value (V_0), then $pI = cV_0$. Using this relationship in the equation $dV/dt = (1-\varepsilon)pI - cV$, where ε is the effectiveness in blocking virion production, yields $dV/dt = (1-\varepsilon)\,cV_0 - cV$, $V(0) = V_0$ with the solution $V(t) = V_0(1-\varepsilon+\varepsilon e^{-ct})$. Because the log change of viral load at time [$\log \Delta V(t)$] equals $\log V(t)/V_0$, the solved equation [$\log \Delta V(t) = \log(1-\varepsilon+\varepsilon e^{-ct})$] was fitted to the values obtained in this study via non-linear least-squares regression in order to estimate ε and c.

ACKNOWLEDGEMENTS

We thank Drs Ichimaro Yamada, Mitsubishi Tanabe Pharma Corporation, and Ann D Kwong, Gururaj Kalkeri, Susan Almquist, Steven M. Lyons and John Randle, Vertex Pharmaceuticals, for their thoughtful discussions. This work was supported in part by Grants-in-Aid for scientific research and development from the Ministry of Education, Sports, Culture and Technology and the Ministry of Health, Labour and Welfare, Japan.

REFERENCES

Boonstra, A., van der Laan, L. J. W., Vanwolleghem, T., Harry, L. A. & Janssen, H. L. A. (2009). Experimental models for hepatitis C viral infection. *Hepatology* **50**, 1646–1655.

Chang, M., Williams, O., Mittler, J., Quintanilla, A., Carithers, R. L., Jr, Perkins, J., Corey, L. & Gretch, D. R. (2003). Dynamics of hepatitis C virus replication in human liver. *Am J Pathol* **163**, 433–444.

Dahari, H., Feliu, A., Garcia-Retortillo, M., Forns, X. & Neumann, A. U. (2005). Second hepatitis C replication compartment indicated by viral dynamics during liver transplantation. *J Hepatol* **42**, 491–498.

Forestier, N., Reesink, H. W., Weegink, C. J., McNair, L., Kieffer, T. L., Chu, H.-M., Purdy, S., Jansen, P. L. M. & Zeuzem, S. (2007). Antiviral

activity of telaprevir (VX-950) and peginterferon alfa-2a in patients with hepatitis C. *Hepatology* **46**, 640–648.

Fried, M. W., Shiffman, M., Reddy, K. R., Smith, C., Marinos, G., Gonçales, F. L., Jr, Häussinger, D., Diago, M., Carosi, G. & other authors (2002). Peginterferon alfa-2a plus ribavirin for chronic hepatitis C virus infection. *N Engl J Med* **347**, 975–982.

Herrmann, E., Lee, J.-H., Marinos, G., Modi, M. & Zeuzem, S. (2003). Effect of ribavirin on hepatitis C viral kinetics in patients treated with pegylated interferon. *Hepatology* **37**, 1351–1358.

Hézode, C., Forestier, N., Dusheiko, G., Ferenci, P., Pol, S., Goeser, T., Bronowicki, M., Bourlière, J.-P., Gharakhanian, S. & other authors (2009). Telaprevir and peginterferon with or without ribavirin for chronic HCV infection. *N Engl J Med* **360**, 1839–1850.

Hiraga, N., Imamura, M., Tsuge, M., Noguchi, C., Takahashi, S., Iwao, E., Fujimoto, Y., Abe, H., Maekawa, T. & other authors (2007). Infection of human hepatocyte chimeric mouse with genetically engineered hepatitis C virus and its susceptibility to interferon. *FEBS Lett* **581**, 1983–1987.

Katoh, M., Sawada, T., Soeno, Y., Nakajima, M., Tateno, C., Yoshizato, K. & Yokoi, T. (2007). *In vivo* drug metabolism model for human cytochrome P450 enzyme using chimeric mice with humanized liver. *J Pharm Sci* **96**, 428–437.

Katoh, M., Tateno, C., Yoshizato, K. & Yokoi, T. (2008). Chimeric mice with humanized liver. *Toxicology* **246**, 9–17.

Kimura, T., Imamura, M., Hiraga, N., Hatakeyama, T., Miki, D., Noguchi, C., Mori, N., Tsuge, M., Takahashi, S. & other authors (2008). Establishment of an infectious genotype 1b hepatitis C virus clone in human hepatocyte chimeric mice. *J Gen Virol* **89**, 2108–2113.

Kneteman, N. M., Weiner, A. J., O'Connell, J., Collett, M., Gao, T., Aukerman, L., Kovelsky, R., Ni, Z.-J., Hashash, A. & other authors (2006). Anti-HCV therapies in chimeric *scid*-Alb/uPA mice parallel outcomes in human clinical application. *Hepatology* **43**, 1346–1353.

Kneteman, N. M., Howe, A. Y. M., Gao, T., Lewis, J., Pevear, D., Lund, G., Douglas, D., Mercer, D. F., Tyrrell, D. L. J. & other authors (2009). HCV796: a selective nonstructural protein 5B polymerase inhibitor with potent anti-hepatitis C virus activity *in vitro*, in mice with chimeric human livers, and in humans infected with hepatitis C virus. *Hepatology* **49**, 745–752.

Lauer, G. M. & Walker, B. D. (2001). Hepatitis C virus infection. *N Engl J Med* **345**, 41–52.

Liang, T. J., Rehermann, B., Seeff, L. B. & Hoofnagle, J. H. (2000). Pathogenesis, natural history, treatment and prevention of hepatitis C. *Ann Intern Med* **132**, 296–305.

Lindenbach, B. D., Meuleman, P., Ploss, A., Vanwolleghem, T., Syder, A. J., McKeating, J. A., Lanford, R. E., Feinstone, S. M., Major, M. E. & other authors (2006). Cell culture-grown hepatitis C virus is infectious *in vivo* and can be recultured *in vitro*. *Proc Natl Acad Sci U S A* **103**, 3805–3809.

Lohmann, V., Körner, F., Koch, J., Herian, U., Theilmann, L. & Bartenschlager, R. (1999). Replication of subgenomic hepatitis C virus RNAs in a hepatoma cell line. *Science* **285**, 110–113.

Manns, M. P., McHutchison, J. G., Gordon, S. C., Rustgi, V. K., Shiffman, M., Reindollar, R., Goodman, Z. D., Koury, K., Ling, M.-H. & other authors (2001). Peginterferon alfa-2b plus ribavirin compared with interferon alfa-2b plus ribavirin for initial treatment of chronic hepatitis C: a randomised trial. *Lancet* **358**, 958–965.

Manns, M. P., Foster, G. R., Rockstroh, J. K., Zeuzem, S., Zoulim, F. & Houghton, M. (2007). The way forward in HCV treatment – finding the right path. *Nat Rev Drug Discov* **6**, 991–1000.

McHutchison, J. G., Everson, G. T., Gordon, S. C., Jacobson, I. M., Sulkowski, M., Kauffman, R., McNair, L., Alam, J., Muir, A. J. & other authors (2009). Telaprevir with peginterferon and ribavirin for chronic HCV genotype 1 infection. *N Engl J Med* **360**, 1827–1838.

Mercer, D. F., Schiller, D. E., Elliott, J. F., Douglas, D. N., Hao, C., Rinfret, A., Addison, W. R., Fischer, K. P., Churchill, T. A. & other authors (2001). Hepatitis C virus replication in mice with chimeric human livers. *Nat Med* **7**, 927–933.

Neumann, A. U., Lam, N. P., Dahari, H., Gretch, D. R., Wiley, T. E., Layden, T. J. & Perelson, A. S. (1998). Hepatitis C viral dynamics *in vivo* and the antiviral efficacy of interferon-α therapy. *Science* **282**, 103–107.

Pawlotsky, J.-M., Dahari, H., Neumann, A. U., Hezode, C., Germanidis, G., Lonjon, I., Castera, L. & Dhumeaux, D. (2004). Antiviral action of ribavirin in chronic hepatitis C. *Gastroenterology* **126**, 703–714.

Pereira, A. A. & Jacobson, I. M. (2009). New and experimental therapies for HCV. *Nat Rev Gastroenterol Hepatol* **6**, 403–411.

Perelson, A. S. & Ribeiro, R. M. (2008). Estimating drug efficacy and viral dynamic parameters: HIV and HCV. *Stat Med* **27**, 4647–4657.

Perni, R. B., Almquist, S. J., Byrn, R. A., Chandorkar, G., Chaturvedi, P. R., Courtney, L. F., Decker, C. J., Dinehart, K., Gates, C. A. & other authors (2006). Preclinical profile of VX-950, a potent, selective, and orally bioavailable inhibitor of hepatitis C virus NS3-4A serine protease. *Antimicrob Agents Chemother* **50**, 899–909.

Powers, K. A., Ribeiro, R. M., Patel, K., Pianko, S., Nyberg, L., Pockros, P., Conrad, A. J., McHutchison, J. & Perelson, A. S. (2006). Kinetics of hepatitis C virus reinfection after liver transplantation. *Liver Transpl* **12**, 207–216.

Poynard, T., Yuen, M.-F., Ratziu, V. & Lai, C. L. (2003). Viral hepatitis C. *Lancet* **362**, 2095–2100.

Quinkert, D., Bartenschlager, R. & Lohmann, V. (2005). Quantitative analysis of the hepatitis C virus replication complex. *J Virol* **79**, 13594–13605.

Ramratnam, B., Bonhoeffer, S., Binley, J., Hurley, A., Zhang, L., Mittler, J. E., Minarkowitz, M., Moore, J. P., Perelson, A. S. & Ho, D. D. (1999). Rapid production and clearance of HIV-1 and hepatitis C virus assessed by large volume plasma apheresis. *Lancet* **354**, 1782–1785.

Reesink, H. W., Zeuzem, S., Weegink, C. J., Forestier, N., Vliet, A., van de Wetering de Rooij, J., McNair, L., Purdy, S., Kauffman, R. & other authors (2006). Rapid decline of viral RNA in hepatitis C patients treated with VX-950: a phase Ib, placebo-controlled, randomized study. *Gastroenterology* **131**, 997–1002.

Sarrazin, C., Kieffer, T. L., Bartels, D., Hanzelka, B., Möh, U., Welker, M., Wincheringer, D., Zhou, Y., Chu, H.-M. & other authors (2007). Dynamic hepatitis C virus genotypic and phenotypic changes in patients treated with the protease inhibitor telaprevir. *Gastroenterology* **132**, 1767–1777.

Schiano, T. D., Gutierrez, J. A., Walewski, J. L., Fiel, M. I., Cheng, B., Bodenheimer, H., Jr, Thung, S. N., Chung, R. T., Schwartz, M. E. & other authors (2005). Accelerated hepatitis C virus kinetics but similar survival rates in recipients of liver grafts from living versus deceased donors. *Hepatology* **42**, 1420–1428.

Sherman, K. E., Fleischer, R., Laessig, K., Murray, J., Tauber, W. & Birnkrant, D. (2007). Development of novel agents for the treatment of chronic hepatitis C infection: summary of the FDA antiviral products advisory committee recommendations. *Hepatology* **46**, 2014–2020.

Talal, A. H., Ribeiro, R. M., Powers, K. A., Grace, M., Cullen, C., Hussain, M., Markatou, M. & Perelson, A. S. (2006). Pharmacodynamics of PEG-IFN α differentiate HIV/HCV coinfected sustained virological responders from nonresponders. *Hepatology* **43**, 943–953.

Tateno, C., Yoshizane, Y., Saito, N., Kataoka, M., Utoh, R., Yamasaki, C., Tachibana, A., Soeno, Y., Asahina, K. & other authors (2004). Near completely humanized liver in mice shows human-type metabolic responses to drugs. *Am J Pathol* **165**, 901–912.

Tsuge, M., Hiraga, N., Takaishi, H., Noguchi, C., Oga, H., Imamura, M., Takahashi, S., Iwao, E., Fujimoto, Y. & other authors (2005). Infection of human hepatocyte chimeric mouse with genetically engineered hepatitis B virus. *Hepatology* **42**, 1046–1054.

Vanwolleghem, T., Meuleman, P., Libbrecht, L., Roskams, T., De Vos, R. & Leroux-Roels, G. (2007). Ultra-rapid cardiotoxicity of the hepatitis C virus protease inhibitor BILN 2061 in the urokinase-type plasminogen activator mouse. *Gastroenterology* **133**, 1144–1155.

Vona, G., Tuveri, R., Delpuech, O., Vallet, A., Canioni, D., Ballardini, G., Trabut, J. B., Le Bail, B., Nalpas, B. & other authors (2004). Intrahepatic hepatitis C virus RNA quantification in microdissected hepatocytes. *J Hepatol* **40**, 682–688.

Wasley, A. & Alter, M. J. (2000). Epidemiology of hepatitis C: geographic differences and temporal trends. *Semin Liver Dis* **20**, 1–16.

Biochemical and Biophysical Research Communications 391 (2010) 316–321

Contents lists available at ScienceDirect

Biochemical and Biophysical Research Communications

journal homepage: www.elsevier.com/locate/ybbrc

Suppression of type I collagen production by microRNA-29b in cultured human stellate cells

Tomohiro Ogawa [a], Masashi Iizuka [a], Yumiko Sekiya [a,b], Katsutoshi Yoshizato [a,c], Kazuo Ikeda [d], Norifumi Kawada [a,*]

[a] Department of Hepatology, Graduate School of Medicine, Osaka City University, Osaka, Japan
[b] Toray Industries Inc., Kanagawa, Japan
[c] PhoenixBio Co. Ltd., Hiroshima, Japan
[d] Department of Functional Anatomy, Graduate School of Medicine, Nagoya City University, Aichi, Japan

ARTICLE INFO

Article history:
Received 6 November 2009
Available online 12 November 2009

Keywords:
Liver fibrosis
SP1
TGF-β
Interferon
TargetScan

ABSTRACT

MicroRNAs (miRNAs) are small noncoding RNAs that regulate gene expression through imperfect base pairing with the 3′ untranslated region (3′UTR) of target mRNA. We studied the regulation of alpha 1 (I) collagen (Col1A1) expression by miRNAs in human stellate cells, which are involved in liver fibrogenesis. Among miR-29b, -143, and -218, whose expressions were altered in response to transforming growth factor-β1 or interferon-α stimulation, miR-29b was the most effective suppressor of type I collagen at the mRNA and protein level via its direct binding to Col1A1 3′UTR. miR-29b also had an effect on SP1 expression. These results suggested that miR-29b is involved in the regulation of type I collagen expression by interferon-α in hepatic stellate cells. It is anticipated that miR-29b will be used for the regulation of stellate cell activation and lead to antifibrotic therapy.

Introduction

Hepatic stellate cells, which reside in the Disse's space outside the liver sinusoids, maintain a quiescent phenotype and store vitamin A under physiological conditions [1,2]. When liver injury occurs due to alcohol abuse, hepatitis viral infection, or obesity, stellate cells activate in response to inflammatory stimuli and become myofibroblastic cells that express smooth muscle α-actin as a representative marker [2]. Myofibroblastic cells secrete profibrogenic mediators, such as transforming growth factor-β (TGF-β), connective tissue growth factor, and tissue inhibitor of matrix metalloproteinases, and generate extracellular matrix materials including collagens, fibronectin, and laminin; thus, they play a pivotal role in liver fibrogenesis [3]. In particular, collagen production by activated stellate cells is regulated by TGF-β in an autocrine loop, which is accompanied by the induction of TGF-β receptors [4]. Suppression of hepatic stellate cell activation and collagen expression is thus a critical issue to establish therapeutic strategies for human liver fibrosis [1,5].

MicroRNAs (miRNAs) are endogenous small noncoding RNAs that modulate gene expression through imperfect base pairing with the 3′ untranslated region (UTR) of target mRNA, resulting in the inhibition of translation or the promotion of mRNA degradation [6,7]. miRNAs play roles in cell proliferation [8], development [9], and differentiation [10], and their contribution to human diseases such as cancer, cardiomyopathies, and schizophrenia have been reported [11–13]. miR-122 is also involved in the defense system against viral hepatitis C with regard to interferon (IFN)-β therapy [14], and miR-26 expression status is associated with survival and response to adjuvant IFNα therapy in patients with hepatocellular carcinoma [15]. Some miRNAs are involved in liver development and hepatocyte lipid metabolism [16–18].

Recent studies have shown that miRNAs are additionally involved in the alteration of hepatic stellate cell phenotypes; down-regulation of miR-27a and -27b allows culture-activated rat stellate cells to return to a quiescent phenotype with abundant vitamin A storage and decreased cell proliferation [19]; miR-15b and -16, which target the Bcl-2 and caspase signaling pathways, may affect stellate cell activation and liver fibrosis [20]. However, the function of miRNAs in hepatic stellate cell activation and their collagen production is largely unknown.

Here, we show that miR-29b, which is induced in human stellate cells (LX-2) treated with IFNα, is a potential regulator of type I collagen mRNA and protein expression. Although the primary action of IFNs is to eradicate viruses, i.e., hepatitis B and C viruses in

Abbreviations: Col1A1, alpha 1 (I) collagen; DMEM, Dulbecco's modified Eagle's medium; FBS, fetal bovine serum; IFN, interferon; miRNAs, microRNAs; TGF-β, transforming growth factor-β; UTR, untranslated region.

* Corresponding author. Address: Department of Hepatology, Graduate School of Medicine, Osaka City University, 1-4-3, Asahimachi, Abeno, Osaka 545-8585, Japan. Fax: +81 6 6646 9072.
E-mail address: kawadanori@med.osaka-cu.ac.jp (N. Kawada).

0006-291X/$ - see front matter © 2009 Elsevier Inc. All rights reserved.
doi:10.1016/j.bbrc.2009.11.056

the case of the liver, IFNs also exhibit an antifibrotic action in human chronic hepatitis [21,22] and rodent liver fibrosis models [23]. Our data suggest that miR-29b may be a novel regulator of type I collagen expression in addition to its involvement in the well-known Smad cascade. Moreover, miR-29b upregulation may play a partial role in the antifibrotic action of IFNs.

Materials and methods

Materials. Recombinant human TGF-β1 was purchased from PeproTech (London, UK). Human natural IFNα was obtained from Otsuka Pharmaceutical Co. (Tokushima, Japan). Precursors of miR-29b, -143, and -218, and the negative control were purchased from Ambion (Austin, TX, USA). Dulbecco's modified Eagle's medium (DMEM) and fetal bovine serum (FBS) were purchased from Sigma Chemical Co. (St. Louis, MO, USA). Rabbit monoclonal antibodies against Smad2 and phospho-Smad2 were purchased from Cell Signaling Technology Inc. (Beverly, MA, USA). The mouse monoclonal antibody against SP1 was purchased from Bio Matrix Research Inc. (Chiba, Japan). Rabbit polyclonal antibody against type I collagen was purchased from Rockland Immunochemicals, Inc. (Gilbertsville, PA, USA). Mouse monoclonal antibody against GAPDH was purchased from Chemicon International Inc. (Temecula, CA, USA). Enhanced Chemiluminescence plus detection reagent was purchased from GE Healthcare (Buckinghamshire, UK). Immobilon P membranes were purchased from Millipore Corp. (Bedford, MA, USA). All other reagents were purchased from Sigma Chemical Co. or Wako Pure Chemical Co. (Osaka, Japan).

Preparation of the human hepatic stellate cell line LX-2. The human hepatic stellate cell line (LX-2, donated by Dr. Scott Friedman), which was spontaneously immortalized by growth in low serum, was established as reported previously [24]. Characterizations of the cells are described in detail elsewhere. The cells were maintained on plastic culture plates in DMEM supplemented with 10% FBS. After the culture had continued for the indicated number of days, the medium was replaced with DMEM supplemented with 0.1% FBS plus test agents, and the culture was continued for another 24 h.

Quantitative real-time PCR. Total RNA was extracted from human stellate cells using the miRNeasy Mini Kit (Qiagen, Valencia, CA, USA). cDNAs were synthesized using 0.5 μg of total RNA, ReverTra Ace (Toyobo, Osaka, Japan), and oligo(dT)$_{12-18}$ primers according to the manufacturer's instructions [25]. Gene expression was measured by real-time PCR using cDNA, real-time PCR Master Mix Reagents (Toyobo), and a set of gene-specific oligonucleotide primers (alpha 1 (I) collagen [Col1A1]: Forward 5′-CCCGGGTTTCAGAGACA ACTTC-3′, Reverse 5′-TCCACATGCTTTATTCCAGCAATC-3′; TGF-β1: Forward 5′-AGCGACTCGCCAGAGTGGTTA-3′, Reverse 5′-GCAGTG TGTTATCCCTGCTGTCA-3′; SP1: Forward 5′-TCGGATGAGCTACA GAGGCACAA-3′, Reverse 5′-GTCACTCCTCATGAAGCGCTTAGG-3′; and GAPDH: Forward 5′-GCACCGTCAAGGCTGAGAAC-3′, Reverse 5′-TGGTGAAGACGCCAGTGGA-3′) with an Applied Biosystems Prism 7500 (Applied Biosystems, Foster City, CA, USA). To detect miRNA expression, the RT reaction was performed using the TaqMan MicroRNA Assay (Applied Biosystems) according to the manufacturer's instructions. The GAPDH level was measured and used to normalize the relative abundance of mRNAs and miRNAs.

Immunoblot. Proteins (20–50 μg) were subjected to sodium dodecyl sulfate–polyacrylamide gel electrophoresis and then transferred onto Immobilon P membranes. After blocking, the membranes were treated with primary antibodies, followed by peroxidase-conjugated secondary antibodies. Immunoreactive bands were visualized by the enhanced chemiluminescence system using the Fujifilm Image Reader LAS-3000 (Fuji Medical Systems, Stamford, CT, USA).

Transient transfection of miRNA precursors. Precursors of miR-29b, -143, and -218, and the negative control were transfected into human stellate cells using Lipofectamine 2000 (Invitrogen, Carlsbad, CA, USA) at a final concentration of 50 nM. Briefly, the cells were plated in DMEM supplemented with 10% FBS at a density of 1–2 × 10^5 cells/ml 24 h prior to the transfection. miRNA precursors and Lipofectamine 2000 were mixed at a ratio of 25 (pmol):1 (μl) in Opti-MEM I Reduced Medium (Invitrogen) and incubated for 20–30 min at room temperature. The miRNA precursor–Lipofectamine 2000 complexes were then added to stellate cell culture medium. After 6 h, the culture medium was changed, and TGF-β1 was added at a concentration of 2 ng/ml.

Luciferase reporter assay. 3′UTRs containing putative miRNA target regions of the Col1A1 and SP1 genes were obtained by PCR using human stellate cell cDNA as a template and primer sets as follows: Col1A1–miR-29: Forward 5′-TTCTCGAGGTTCTTGTCTTG ATGTGTCACC-3′, Reverse 5′-TTTCTAGAGAGAGCAGAGGCCTGAGA AG-3′; Col1A1–miR-143: Forward 5′-CTCGAGACTCCCTCCATCCCAA CCT-3′, Reverse 5′-TCTAGAATTGCTGGGCAGACAATAC-3′; Col1A1–miR-218: Forward 5′-CTCGAGGTGGATGGGGACTTGTGAAT-3′, Reverse 5′-TCTAGATTATGTTTGGGTCATTTCCAC-3′; SP1–miR-29: Forward 5′-TTCTCGAGTGGGTGCTACACAGAATGC-3′, Reverse 5′-TTTC TAGAAGACTGTCCTTATTTCCTTGGTA-3′; and SP1–miR-218: Forward 5′-CTCGAGGATGTTTTCCCTTAACTTTTCCT-3′, Reverse 5′-TCT AGACTAAAAGCTTATATCCTCAGCATC-3′. Each of the forward and reverse primers carried the *Xho*I and *Xba*I sites at their 5′-ends. The obtained DNA fragments were inserted into the pmirGLO Vector (Promega, San Luis Obispo, CA, USA). The resulting vectors were dubbed pCol1A1–miR-29/mirGLO, pCol1A1–miR-143/mirGLO, pCol1A1–miR-218/mirGLO, pSP1–miR-29/mirGLO, and pSP1–miR-218/mirGLO. Human stellate cells were seeded on 96-well plates (Microtest 96-well Assay Plate; Becton Dickinson, Franklin Lakes, NJ, USA) in DMEM supplemented with 10% FBS at a density of 2 × 10^4 cells/well. The following day, they were transfected with 200 ng of reporter plasmid along with miRNA precursors using Lipofectamine 2000 as described above and incubated for an additional 24 h. After incubation, the medium was removed from the wells, and 20 μl of phosphate-buffered saline was added. The Dual-Glo Luciferase Assay System (Promega) was used to analyze luciferase expression according to the manufacturer's protocol. Firefly luciferase activity was normalized to *Renilla* luciferase activity to adjust for variations in transfection efficiency among experiments.

Statistical analysis. Data presented as bar graphs are the means ± SD of at least three independent experiments. Statistical analysis was performed using Student's *t*-test, and $P < 0.05$ was considered significant.

Results and discussion

Regulation of Col1A1 expression by TGF-β1 and IFNα in human stellate cells

Immortalized human stellate cells, LX-2, are classified as an activated phenotype that expresses mRNAs for Col1A1 and other fibrogenetic molecules and are reported to be highly gene-transfectable [24]. At first, we observed that Col1A1 mRNA expression increased dose-dependently by TGF-β1 (Fig. 1A), whereas this upregulation was significantly inhibited by the presence of 100 IU/ml of human IFNα (Fig. 1B).

Extraction of miR-29b, -143, and -218 as candidates interacting with Col1A1 3′UTR

To determine the role of miRNAs in human stellate cell collagen expression, we searched for predictable miRNAs that could interact

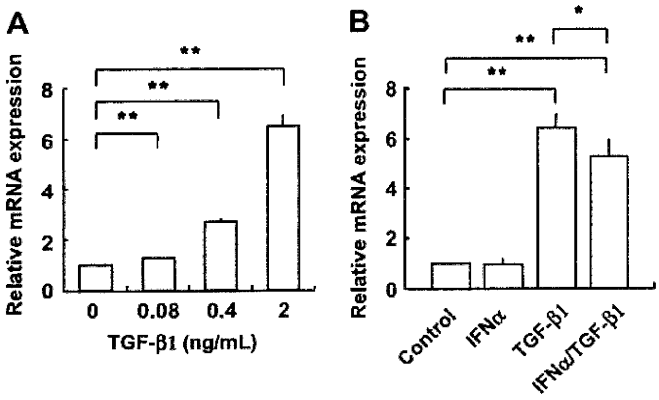

Fig. 1. Regulation of alpha 1 (I) collagen (Col1A1) expression in human stellate cells. (A) Dose-dependent effect of TGF-β1 on Col1A1 mRNA expression. Human stellate cells, LX-2, were treated with TGF-β1 (0, 0.08, 0.4, and 2 ng/ml) for 24 h in DMEM containing 0.1% FBS. (B) Effect of IFNα on Col1A1 mRNA expression in human stellate cells stimulated with TGF-β1. The cells were treated with IFNα (100 IU/ml), TGF-β1 (2 ng/ml), or IFNα (100 IU/ml) + TGF-β1 (2 ng/ml) for 24 h in DMEM containing 0.1% FBS. Control: human stellate cells were cultured for 24 h in DMEM containing 0.1% FBS. mRNA expression was analyzed by real-time PCR. The results are expressed as relative expression against control expression without treatment. $^{*}P < 0.05$; $^{**}P < 0.01$.

with 3′UTR of human Col1A1 mRNA using TargetScan Human Release 5.1 (http://www.targetscan.org/). As a result, miR-29, -98, -129, -133, -143, -196, -218, and let-7 were extracted as candidates. Because further *in silico* analyses among the eight candidates indicated that miR-29b, -143, and -218 were highly homologous to the Col1A1 3′UTR, we checked the expression levels of these miRNAs in human stellate cells by real-time PCR. As a result, miR-143 and -218 expressions were up and downregulated dose-dependently by TGF-β1, respectively, (Fig. 2A and B). Although miR-29b expression was unaffected by TGF-β1, it increased in

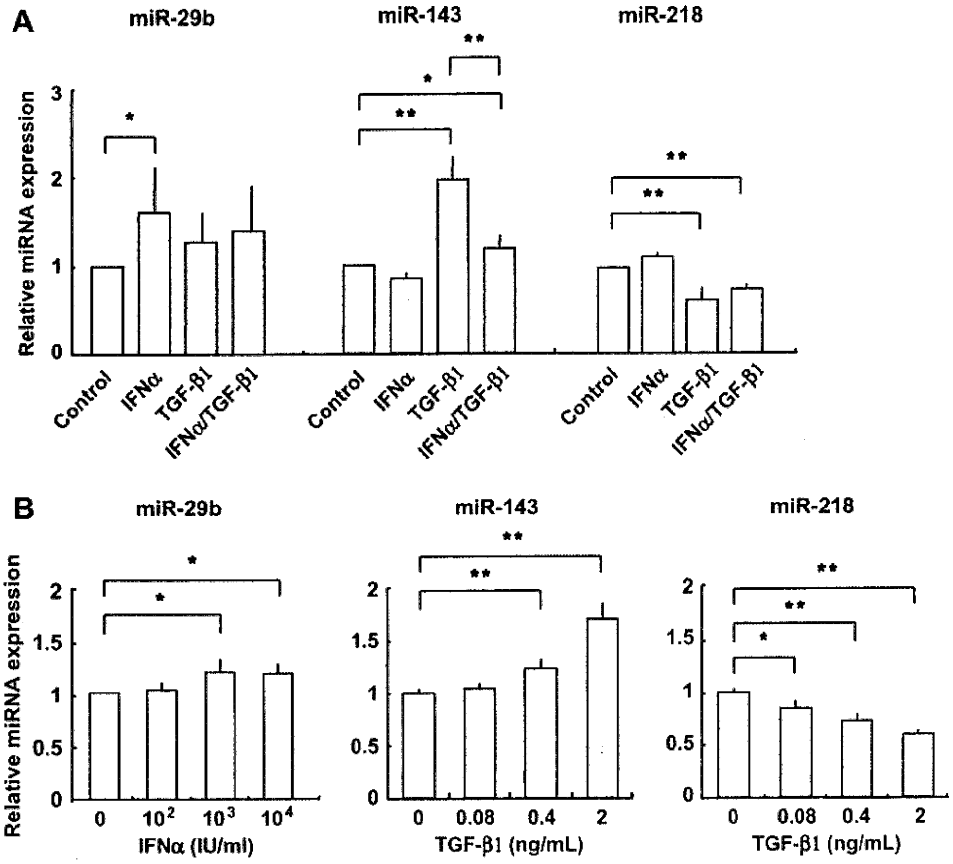

Fig. 2. Expression of miR-29b, -143, and -218 in human stellate cells. (A) Expression of miR-29b, -143, and -218 in human stellate cells, LX-2. The cells were treated with IFNα (100 IU/ml), TGF-β1 (2 ng/ml), or IFNα (100 IU/ml) + TGF-β1 (2 ng/ml) for 24 h in DMEM containing 0.1% FBS. Control: human stellate cells were cultured for 24 h in DMEM containing 0.1% FBS. (B) Dose-dependent effect of IFNα or TGF-β1 on the expression of miR-29b, -143, and -218 in human stellate cells. miRNA expression was analyzed by real-time PCR. The results are expressed as relative expression against control expression without treatment. $^{*}P < 0.05$; $^{**}P < 0.01$.

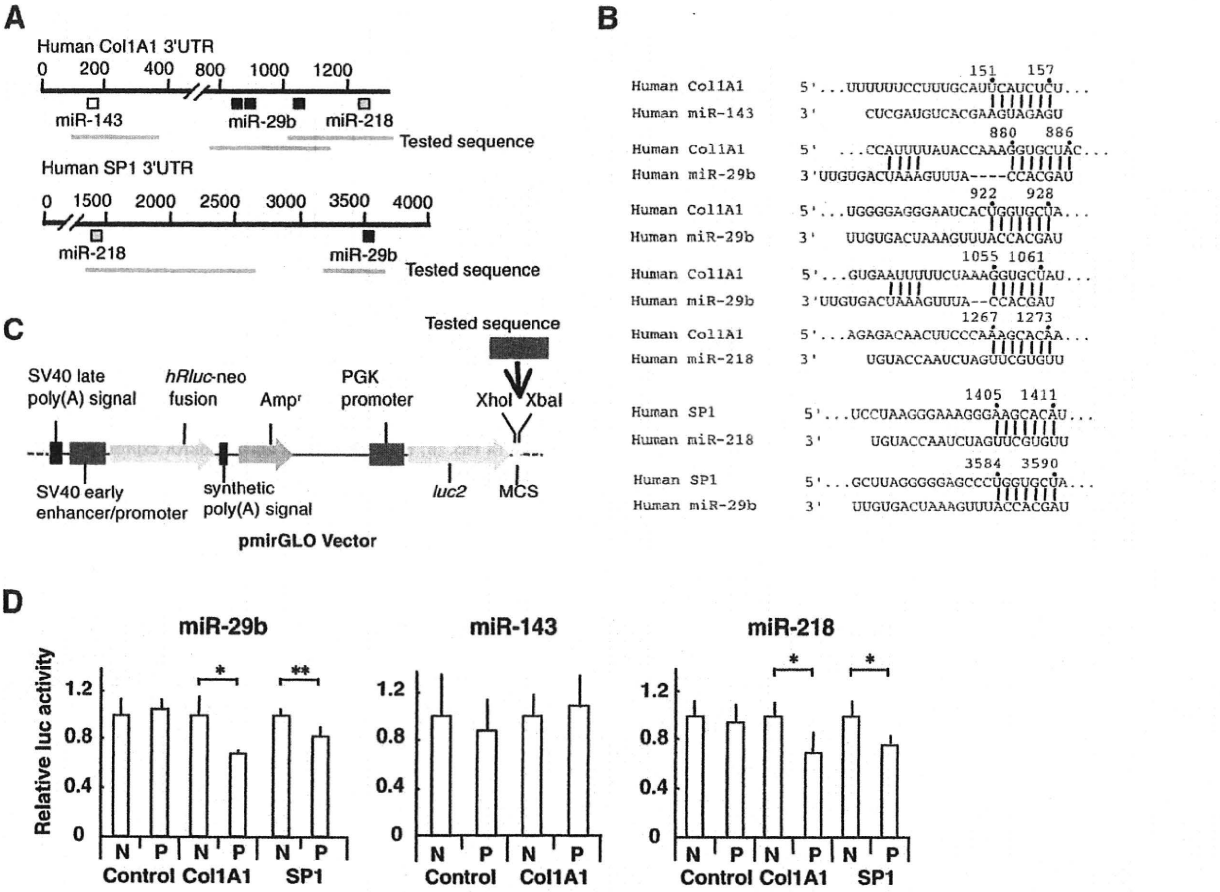

Fig. 3. Interaction of miR-29b, -143, and -218 with the 3′UTRs of alpha 1 (I) collagen (Col1A1) and SP1 mRNAs. (A) Schematic indication of the miRNA binding sites in the 3′UTRs of Col1A1 and SP1 mRNAs based on TargetScan Human Release 5.1 (http://www.targetscan.org/). Each black, white, and gray box indicates miR-29b, -143, and -218, respectively. Tested sequences indicate the regions that were inserted into the luciferase reporter vector. (B) Predicted consequential pairing of the target region and miRNAs. Arabic numerals above indicate the positions relative to the 3′UTR start sites. (C) Luciferase reporter vector structure. The vector contained two expression units; one for the *Renilla* luciferase gene (*hRluc*-neo fusion) expression. This unit was driven by an SV40 early promoter. The other was for the firefly luciferase gene (*luc2*). This unit was driven by a human phosphoglycerate kinase (PGK) promoter and contained multiple cloning sites (MCS) downstream of the *luc2* sequence. Each Col1A1 and SP1 3′UTR containing a putative miRNA target region (tested sequence) was cloned into the MCS. Arrows indicate the gene directions. Amp^R indicates an ampicillin-resistant plasmid gene. (D) Interaction of miR-29b, -143, and -218 with the 3′UTRs of Col1A1 and SP1 mRNAs in human stellate cells. Relative luciferase activity derived from pCol1A1–miR-29/mirGLO and pSP1–miR-29/mirGLO in the presence of miR-29b precursors (left panel), pCol1A1–miR-143/mirGLO in the presence of miR-143 precursors (center panel), and pCol1A1–miR-218/mirGLO and pSP1–miR-218/mirGLO in the presence of miR-218 precursors (right panel). The pmirGLO vector was used as a negative control reporter vector (control). N: cotransfection of reporter vectors along with negative control precursors, which have a scrambled sequence. P: cotransfection of reporter vectors along with miRNA precursors. Firefly and *Renilla* luciferase activities were determined, and firefly luciferase was normalized to *Renilla* luciferase activity. Results are expressed as relative activities against the activity in the presence of negative control precursors. $^{*}P < 0.05$ and $^{**}P < 0.01$.

the presence of IFNα (Fig. 2A and B). Thus, we assumed that these miRNAs might affect type I collagen expression via their interaction with Col1A1 3′UTR in human stellate cells.

Interaction of miR-29b, -143, and -218 with 3′UTRs of Col1A1 and SP1 mRNAs

The prediction of miRNA target regions on Col1A1 3′UTR by TargetScan indicated that Col1A1 3′UTR has three target regions for miR-29b, one for miR-143, and one for miR-218 (Fig. 3A and B). Because collagen gene expression is regulated by miR-192 via an interaction with the transcriptional repressor E-box [26], we additionally considered SP1, which is a transcriptional regulator of Col1A1 expression induced by TGF-β1 [27,28]. The predicted miRNA target regions of SP1 3′UTR contained one target region for miR-29b and one for miR-218 (Fig. 3A and B).

To investigate the direct targeting of Col1A1 by miR-29b, -143, and -218 and that of SP1 by miR-29b and -218, the sequence of each target region was cloned and inserted into the downstream region of the firefly luciferase reporter gene (Fig. 3C). The resulting vectors were dubbed pCol1A1–miR-29/mirGLO, pCol1A1–miR-143/mirGLO, pCol1A1–miR-218/mirGLO, pSP1–miR-29/mirGLO, and pSP1–miR-218/mirGLO. These vectors were cotransfected into human stellate cells with miRNA precursors. As a result, the miR-29b and -218 precursors inhibited luciferase activity derived from the vectors carrying Col1A1 or SP1 3′UTRs (Fig. 3D). In contrast, the miR-143 precursors had no effect on luciferase activity of the vector carrying Col1A1 3′UTR (Fig. 3D). According to these observations, we assumed that the Col1A1 and SP1 3′UTR sequences could be targeted by miR-29b and -218, whereas miR-143, which was induced by TGF-β1 (Fig. 2A and B), had a negligible effect on Col1A1 expression in human stellate cells.

Regulation of type I collagen expression by miR-29b and -218

Next, we examined the effect of miR-29b and -218 overexpression on type I collagen mRNA and protein expression in human stellate cells. Transient transfection of miR-29b precursors signifi-

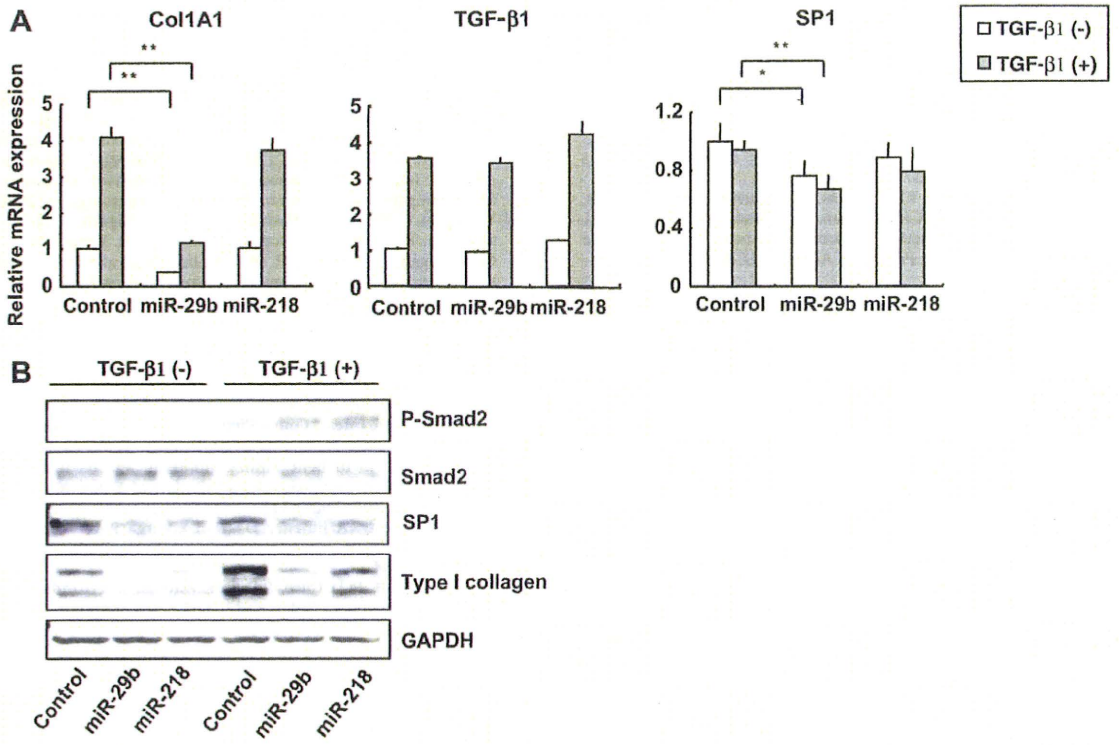

Fig. 4. Effect of miR-29b and -218 on type I collagen expression in human stellate cells. Human stellate cells were cultured in DMEM supplemented with 10% FBS and were transfected with 50 nM miR-29b, -218 precursors, or a negative control, which had a scrambled sequence (control) using Lipofectamine 2000. After 6 h, the medium was changed to DMEM containing 0.1% FBS with or without 2 ng/ml TGF-β1, and the culture was continued for another 24 h. (A) Effect of miR-29b and -218 precursors on the expression of Col1A1, TGF-β1, and SP1 mRNAs in human stellate cells with (gray column) or without (white column) TGF-β1. mRNA expression was analyzed by real-time PCR. The results are expressed as relative expression against control expression. $^{*}P < 0.05$; $^{**}P < 0.01$. (B) Effect of miR-29b and -218 precursors on the protein expression of phospho-Smad2 (P-Smad2), Smad2, SP1, type I collagen, and GAPDH in human stellate cells in the presence (+) or absence (−) of TGF-β1.

cantly inhibited type I collagen mRNA and protein expression (Fig. 4A, left panel, and B) in unstimulated human stellate cells. Additionally, transfection of miR-29b precursors completely suppressed the upregulation of type I collagen mRNA and protein under TGF-β1 stimulation. TGF-β1 stimulation induces Col1A1 mRNA expression through a pathway that includes SP1 and phosphorylated Smad2/3 [29]. In our results, upregulation of TGF-β1 mRNA (Fig. 4A, center panel) and phosphorylation of Smad2 (Fig. 4B) under TGF-β1 stimulation were unaffected by the transfection of miR-29b precursors. These results suggested that miR-29b may affect the downstream of phosphorylated Smad2. Moreover, the transfection of miR-29b precursors decreased SP1 mRNA and protein expression (Fig. 4A, right panel, and B). Thus, the miR-29b-induced repression of type I collagen expression could be caused by its direct interaction with Col1A1 3′UTR and additionally by its interaction with SP1 expression in human stellate cells. These observations agree with a report showing the role of miR-29 in collagen expression and cardiac fibrosis after cardiac infarction [30]. In contrast, transfection of miR-218 precursors triggered a negligible change in Col1A1 and SP1 mRNA expression (Fig. 4A, left and right panels) but slightly reduced their protein level (Fig. 4B). Taken together, these results imply that miR-29b is the most potent miRNA with regard to collagen production in human stellate cells.

Conclusions

We found a potent repression of collagen production by miR-29b in human stellate cells. IFNs attenuate and may regress liver fibrosis caused by hepatitis C viral infection [21–23], although the precise molecular mechanism has yet to be demonstrated. The present study using human stellate cells demonstrated that IFNα upregulates miR-29b (Fig. 2B and C), which is a negative regulator of type I collagen production via the interaction with Col1A1 and SP1 3′UTRs. This observation implies the contribution of miR-29b to antifibrotic IFN actions. Targeted delivery of miR-29b to activated stellate cells in the liver could become a new therapeutic strategy for human liver fibrosis in the future.

Acknowledgment

This work was supported by a grant from the Ministry of Health, Labour and Welfare of Japan to N. Kawada (2008–2009).

References

[1] R. Bataller, D.A. Brenner, Hepatic stellate cells as a target for the treatment of liver fibrosis, Semin. Liver Dis. 21 (2001) 437–451.
[2] S.L. Friedman, Molecular regulation of hepatic fibrosis, an integrated cellular response to tissue injury, J. Biol. Chem. 275 (2000) 2247–2250.
[3] N. Kawada, The hepatic perisinusoidal stellate cell, Histol. Histopathol. 12 (1997) 1069–1080.
[4] S. Dooley, B. Delvoux, B. Lahme, K. Mangasser-Stephan, A.M. Gressner, Modulation of transforming growth factor beta response and signaling during transdifferentiation of rat hepatic stellate cells to myofibroblasts, Hepatology 31 (2000) 1094–1106.
[5] E. Albanis, S.L. Friedman, Hepatic fibrosis. Pathogenesis and principles of therapy, Clin. Liver Dis. 5 (2001) 315–334. v–vi.
[6] W. Filipowicz, S.N. Bhattacharyya, N. Sonenberg, Mechanisms of post-transcriptional regulation by microRNAs: are the answers in sight?, Nat Rev. Genet. 9 (2008) 102–114.
[7] D.P. Bartel, MicroRNAs: genomics, biogenesis, mechanism, and function, Cell 116 (2004) 281–297.
[8] J. Brennecke, D.R. Hipfner, A. Stark, R.B. Russell, S.M. Cohen, Bantam encodes a developmentally regulated microRNA that controls cell proliferation and regulates the proapoptotic gene hid in *Drosophila*, Cell 113 (2003) 25–36.

[9] G.M. Schratt, F. Tuebing, E.A. Nigh, C.G. Kane, M.E. Sabatini, M. Kiebler, M.E. Greenberg, A brain-specific microRNA regulates dendritic spine development, Nature 439 (2006) 283–289.
[10] C.Z. Chen, L. Li, H.F. Lodish, D.P. Bartel, MicroRNAs modulate hematopoietic lineage differentiation, Science 303 (2004) 83–86.
[11] J. Kota, R.R. Chivukula, K.A. O'Donnell, E.A. Wentzel, C.L. Montgomery, H.W. Hwang, T.C. Chang, P. Vivekanandan, M. Torbenson, K.R. Clark, J.R. Mendell, J.T. Mendell, Therapeutic microRNA delivery suppresses tumorigenesis in a murine liver cancer model, Cell 137 (2009) 1005–1017.
[12] J.F. Chen, E.P. Murchison, R. Tang, T.E. Callis, M. Tatsuguchi, Z. Deng, M. Rojas, S.M. Hammond, M.D. Schneider, C.H. Selzman, G. Meissner, C. Patterson, G.J. Hannon, D.Z. Wang, Targeted deletion of Dicer in the heart leads to dilated cardiomyopathy and heart failure, Proc. Natl. Acad. Sci. USA 105 (2008) 2111–2116.
[13] D.O. Perkins, C.D. Jeffries, L.F. Jarskog, J.M. Thomson, K. Woods, M.A. Newman, J.S. Parker, J. Jin, S.M. Hammond, MicroRNA expression in the prefrontal cortex of individuals with schizophrenia and schizoaffective disorder, Genome Biol. 8 (2007) R27.
[14] I.M. Pedersen, G. Cheng, S. Wieland, S. Volinia, C.M. Croce, F.V. Chisari, M. David, Interferon modulation of cellular microRNAs as an antiviral mechanism, Nature 449 (2007) 919–922.
[15] J. Ji, J. Shi, A. Budhu, Z. Yu, M. Forgues, S. Roessler, S. Ambs, Y. Chen, P.S. Meltzer, C.M. Croce, L.X. Qin, K. Man, C.M. Lo, J. Lee, I.O. Ng, J. Fan, Z.Y. Tang, H.C. Sun, X.W. Wang, MicroRNA expression, survival, and response to interferon in liver cancer, N. Engl. J. Med. 361 (2009) 1437–1447.
[16] C.E. Rogler, L. Levoci, T. Ader, A. Massimi, T. Tchaikovskaya, R. Norel, L.E. Rogler, MicroRNA-23b cluster microRNAs regulate transforming growth factor-beta/bone morphogenetic protein signaling and liver stem cell differentiation by targeting Smads, Hepatology 50 (2009) 575–584.
[17] C. Esau, S. Davis, S.F. Murray, X.X. Yu, S.K. Pandey, M. Pear, L. Watts, S.L. Booten, M. Graham, R. McKay, A. Subramaniam, S. Propp, B.A. Lollo, S. Freier, C.F. Bennett, S. Bhanot, B.P. Monia, MiR-122 regulation of lipid metabolism revealed by in vivo antisense targeting, Cell Metab. 3 (2006) 87–98.
[18] L. Zheng, G.C. Lv, J. Sheng, Y.D. Yang, Effect of miRNA-10b in regulating cellular steatosis level by targeting PPAR-alpha expression, a novel mechanism for the pathogenesis of NAFLD, J. Gastroenterol. Hepatol. (2009).
[19] J. Ji, J. Zhang, G. Huang, J. Qian, X. Wang, S. Mei, Over-expressed microRNA-27a and 27b influence fat accumulation and cell proliferation during rat hepatic stellate cell activation, FEBS Lett. 583 (2009) 759–766.
[20] C.J. Guo, Q. Pan, D.G. Li, H. Sun, B.W. Liu, MiR-15b and miR-16 are implicated in activation of the rat hepatic stellate cell: an essential role for apoptosis, J. Hepatol. 50 (2009) 766–778.
[21] Y. Shiratori, F. Imazeki, M. Moriyama, M. Yano, Y. Arakawa, O. Yokosuka, T. Kuroki, S. Nishiguchi, M. Sata, G. Yamada, S. Fujiyama, H. Yoshida, M. Omata, Histologic improvement of fibrosis in patients with hepatitis C who have sustained response to interferon therapy, Ann. Intern. Med. 132 (2000) 517–524.
[22] T. Poynard, J. McHutchison, G.L. Davis, R. Esteban-Mur, Z. Goodman, P. Bedossa, J. Albrecht, Impact of interferon alfa-2b and ribavirin on progression of liver fibrosis in patients with chronic hepatitis C, Hepatology 32 (2000) 1131–1137.
[23] Y. Inagaki, T. Nemoto, M. Kushida, Y. Sheng, K. Higashi, K. Ikeda, N. Kawada, F. Shirasaki, K. Takehara, K. Sugiyama, M. Fujii, H. Yamauchi, A. Nakao, B. De Crombrugghe, T. Watanabe, I. Okazaki, Interferon alfa down-regulates collagen gene transcription and suppresses experimental hepatic fibrosis in mice, Hepatology 38 (2003) 890–899.
[24] L. Xu, A.Y. Hui, E. Albanis, M.J. Arthur, S.M. O'Byrne, W.S. Blaner, P. Mukherjee, S.L. Friedman, F.J. Eng, Human hepatic stellate cell lines, LX-1 and LX-2: new tools for analysis of hepatic fibrosis, Gut 54 (2005) 142–151.
[25] K. Otogawa, T. Ogawa, R. Shiga, K. Nakatani, K. Ikeda, Y. Nakajima, N. Kawada, Attenuation of acute and chronic liver injury in rats by iron-deficient diet, Am. J. Physiol. Regul. Integr. Comp. Physiol. 294 (2008) R311–R320.
[26] M. Kato, J. Zhang, M. Wang, L. Lanting, H. Yuan, J.J. Rossi, R. Natarajan, MicroRNA-192 in diabetic kidney glomeruli and its function in TGF-beta-induced collagen expression via inhibition of E-box repressors, Proc. Natl. Acad. Sci. USA 104 (2007) 3432–3437.
[27] L. Li, C.M. Artlett, S.A. Jimenez, D.J. Hall, J. Varga, Positive regulation of human alpha 1 (I) collagen promoter activity by transcription factor Sp1, Gene 164 (1995) 229–234.
[28] I. Garcia-Ruiz, P. de la Torre, T. Diaz, E. Esteban, I. Fernandez, T. Munoz-Yague, J.A. Solis-Herruzo, Sp1 and Sp3 transcription factors mediate malondialdehyde-induced collagen alpha 1 (I) gene expression in cultured hepatic stellate cells, J. Biol. Chem. 277 (2002) 30551–30558.
[29] P. Sysa, J.J. Potter, X. Liu, E. Mezey, Transforming growth factor-beta1 up-regulation of human alpha(1) (I) collagen is mediated by Sp1 and Smad2 transacting factors, DNA Cell Biol. 28 (2009) 425–434.
[30] E. van Rooij, L.B. Sutherland, J.E. Thatcher, J.M. DiMaio, R.H. Naseem, W.S. Marshall, J.A. Hill, E.N. Olson, Dysregulation of microRNAs after myocardial infarction reveals a role of miR-29 in cardiac fibrosis, Proc. Natl. Acad. Sci. USA 105 (2008) 13027–13032.

HUMAN GENE THERAPY 21:40–50 (January 2010)

DOI: 10.1089/hum.2009.027

In Vivo Stable Transduction of Humanized Liver Tissue in Chimeric Mice via High-Capacity Adenovirus–Lentivirus Hybrid Vector

Shuji Kubo,[1,2] Miho Kataoka,[3] Chise Tateno,[3] Katsutoshi Yoshizato,[3,4] Yoshiko Kawasaki,[2] Takahiro Kimura,[1] Emmanuelle Faure-Kumar,[1] Donna J. Palmer,[5] Philip Ng,[5] Haruki Okamura,[2] and Noriyuki Kasahara[1]

Abstract

We developed hybrid vectors employing high-capacity adenovirus as a first-stage carrier encoding all the components required for *in situ* production of a second-stage lentivirus, thereby achieving stable transgene expression in secondary target cells. Such vectors have never previously been tested in normal tissues, because of the scarcity of suitable *in vivo* systems permissive for second-stage lentivirus assembly. Here we employed a novel murine model in which endogenous liver tissue is extensively reconstituted with engrafted human hepatocytes, and successfully achieved stable transduction by the second-stage lentivirus produced *in situ* from first-stage adenovirus. This represents the first demonstration of the functionality of adenoviral-lentiviral hybrid vectors in a normal parenchymal organ *in vivo*.

Introduction

ADENOVIRAL VECTORS (AdVs) have been successfully used *in vivo* to transduce various postmitotic tissues, but generally only transient gene expression can be achieved because of cytotoxic T-lymphocyte–mediated immune responses against viral genes retained in conventional AdVs, and their extremely low frequency of chromosomal integration (Harui *et al.*, 1999; Wivel *et al.*, 1999). More persistent expression can be maintained by high-capacity, helper-dependent AdVs (HDAdVs) from which all of the viral coding sequences have been removed (Parks *et al.*, 1996; Schiedner *et al.*, 1998; Kochanek, 1999; Kim *et al.*, 2001; Oka *et al.*, 2001), but its duration is still limited because of progressive dilution of the extrachromosomal HDAdV vector DNA as transduced cells divide. Treatment of hereditary diseases may require more stable, long-term transgene expression, which can be achieved only through permanent integration or ongoing episomal replication of vector DNA.

To overcome this limitation, various hybrid vector systems have been developed, which employ AdV as a first-stage delivery vehicle to efficiently enter target cells, but then utilize the machinery of integrating viruses or mobile genetic elements to achieve permanent chromosomal integration (Feng *et al.*, 1997; Caplen *et al.*, 1999; Lieber *et al.*, 1999; Recchia *et al.*, 1999; Tan *et al.*, 1999; Leblois *et al.*, 2000; Soifer *et al.*, 2001; Soifer *et al.*, 2002; Yant *et al.*, 2002; Kubo and Mitani, 2003; Dorigo *et al.*, 2004; Picard-Maureau *et al.*, 2004). Efficient two-stage transduction *in vitro* and stable long-term transgene expression have previously been demonstrated with AdV–transposon (Soifer *et al.*, 2001; Yant *et al.*, 2002), AdV–adeno-associated virus (Lieber *et al.*, 1999; Recchia *et al.*, 1999), AdV–retrovirus (Feng *et al.*, 1997; Caplen *et al.*, 1999; Soifer *et al.*, 2002), AdV–foamy virus (Picard-Maureau *et al.*, 2004), and AdV–lentivirus (Kubo and Mitani, 2003) vectors. In particular, Kubo and Mitani (2003) have demonstrated the ability of an AdV–lentivirus hybrid vector to efficiently enter a variety of cell types via the first-stage HDAdV and subsequently mediate *in situ* production of a human immunodeficiency virus (HIV)-derived second-stage lentiviral vector (LV), which then stably delivers a marker gene to neighboring cells. However, this hybrid vector generated second-stage LV pseudotyped with the vesicular stomatitis virus G glycoprotein (VSV-G), a highly fusogenic and toxic envelope

[1]Division of Digestive Diseases, Department of Medicine, University of California at Los Angeles, Los Angeles, CA 90095.
[2]Laboratory of Host Defenses, Institute for Advanced Medical Sciences, Hyogo College of Medicine, Nishinomiya, Hyogo 663-8501, Japan.
[3]Yoshizato Project, CLUSTER, Hiroshima Prefectural Institute of Industrial Science and Technology, Higashi-Hiroshima, Hiroshima 739-0046, Japan.
[4]Developmental Biology Laboratory and Hiroshima University 21st Century COE Program for Advanced Radiation Casualty Medicine, Department of Biological Science, Graduate School of Science, Higashi-Hiroshima, Hiroshima 739-8526, Japan.
[5]Center for Cell & Gene Therapy, Baylor College of Medicine, Houston, TX 77030.

protein (Ory *et al.*, 1996), which may result in unwanted cytotoxic effects in the primary target cells during LV production. Further, the ability of AdV-lentivirus hybrid vectors to stably transduce normal quiescent tissues *in vivo* has never previously been tested.

We have now developed an improved high-capacity AdV-lentivirus hybrid vector system, designated HL, and examined the ability of this new hybrid system to mediate efficient and stable gene transfer *in vitro* and *in vivo*. The first-stage HDAdV of the HL hybrid system directs the production of a minimal second-stage LV that retains less than 800 bp of HIV sequence (Chen *et al.*, 2002) and is pseudotyped with the murine leukemia virus (MLV) 4070A amphotropic envelope, which is much less cytotoxic than VSV-G. However, to test the transduction efficiency of the new HL hybrid vector system, target cells that can support *in situ* production of the HIV-derived second-stage LV are required. For *in vitro* experiments, human cell lines permissive for HIV replication can be employed. However, the requirement for human target cells presents a challenge to testing the functionality of the HL hybrid vector system *in vivo*, particularly with respect to its ability to stably transduce normal organs and tissues.

As nearly 90% of the input dose of AdV introduced *in vivo* accumulates in the liver upon intravenous injection (Kass-Eisler *et al.*, 1994; Huard *et al.*, 1995; Kubo *et al.*, 1997), and nearly 100% transduction of hepatocytes can be achieved at higher doses (Li *et al.*, 1993), the liver is an attractive target for *in vivo* testing of the HL system. However, multiple blocks to HIV replication have been reported in rodent cells, including cellular entry, reduced abundance of unspliced HIV-RNA and *gag* proteins, and defects in infectious particle assembly (Hofmann *et al.*, 1999; Bieniasz and Cullen, 2000; Mariani *et al.*, 2000). Therefore, to test the HL hybrid vector *in vivo*, we sought a humanized liver model that is permissive for HIV particle assembly.

Successful reconstitution of human liver tissue has recently been achieved in immunodeficient mice (Dandri *et al.*, 2001; Mercer *et al.*, 2001). Dandri *et al.* (2001) reported that cross-breeding of recombinant activation gene-2–deleted mice with transgenic mice expressing the hepatotoxic urokinase-type plasminogen activator (uPA) results in immunodeficient progeny which undergo progressive liver degeneration. These progeny were successfully transplanted with human hepatocytes, resulting in chimeric liver tissue with a replacement index of up to 15%, rendering these mice permissive for HBV infection (Dandri *et al.*, 2001). Similarly, Mercer *et al.* (2001) demonstrated that uPA/SCID mice bearing chimeric humanized livers with replacement index values of 50% could support HCV replication (Dandri *et al.*, 2001). More extensive repopulation has been difficult to achieve, likely because engrafted human hepatocytes produce complement factors, which appear to exert lethal effects in mice with higher replacement values. However, Tateno *et al.* (2004) and Yoshizato and colleagues (2004) have recently demonstrated that administration of a C5/C3 convertase inhibitor successfully rescued uPA/SCID mice whose chimeric livers proved to be almost completely repopulated with human hepatocytes exhibiting normal cytoarchitecture. The transduction efficiency of oncoretroviral vectors has previously been tested in this humanized liver model, and consistent with their inability to enter quiescent postmitotic cells, was found to be in the order of 5% (Emoto *et al.*, 2005). We have now utilized this unique chimeric liver model to test the ability of the HL hybrid system to mediate efficient entry by the first-stage HDAdV, *in situ* production of the second-stage LV, and stable transduction in fully humanized livers *in vivo*. To our knowledge, this represents the first report of *in vivo* testing of an AdV–lentivirus hybrid vector system in a normal parenchymal organ.

Materials and Methods

Cells

Cell lines including 293 (Graham *et al.*, 1977) (Microbix, Toronto, Canada), 293T (DuBridge *et al.*, 1987), and the Gli36 human glioma (Sena-Esteves *et al.*, 2000) were cultured in Dulbecco's modified Eagle's medium supplemented with 10% fetal calf serum (FCS; Omega, Tarzana, CA). Hep3B human hepatocellular carcinoma cells were cultured in Eagle's minimum essential medium supplemented with 10% FCS, 1 m*M* sodium pyruvate, and nonessential amino acids. Primary human hepatocytes and their specific medium were purchased from Cambrex (Baltimore, MD; CC-2591).

HL first-stage HDAdV construction and production

The phosphoglycerokinase promoter-driven green fluorescence protein (GFP) marker gene cassette, cytomegalovirus promoter (CMV)-driven *gag/pol/rev* lentiviral packaging cassette, simian virus 40 early promoter-driven MLV 4070A amphotropic envelope cassette, and minimal LV construct (Robbins *et al.*, 1998; Chen *et al.*, 2002) were sequentially cloned into the HDAdV plasmid pSTK120, which contains the human Ad5 inverted terminal repeat sequences and packaging signal, resulting in the construction of the complete HL vector plasmid, pHL. Additional details regarding the pHL construct, and the HIV-based minimal LV contained therein, are provided upon request.

The HL vector and control HDAdV cmv-GFP (Ad GFP) were prepared using the FLPe/*FRT* helper virus system (Umana *et al.*, 2001). The vectors were titrated on 293 cells for GFP expression, using a FACScalibur flow cytometer (Becton Dickinson, San Jose, CA), on day 2 post-infection, defined as transducing units per ml (TU/ml). Another control HDAdV, HDΔ28E4LacZ, was prepared as previously described (Palmer and Ng, 2003). Helper virus contamination levels were determined by Southern blot, as previously described (Kubo and Mitani, 2003).

Second-stage LV production after infection with HL first-stage HDAdV

To confirm production of LV in cells (Gli36, HeLa, Hep3B, HepG2 and human primary hepatocytes) infected by the HL vector, 4×10^5 cells of each were infected with various amounts of HL vector. The amount of vector used for each infection was based on the titer determined using each cell line. At 4 hr postinfection, the infected cells were washed three times with phosphate-buffered saline (PBS), and incubated in growth medium. At 48 hr postinfection, the virus-containing medium was harvested, centrifuged, filtered through a 0.45-μm pore filter, and used for titration on 293 cells by X-galactosidase (gal) staining to detect βgal expression. In preliminary experiments, the level of residual adenovirus carried over in the filtered supernatant medium after infection of primary cells at a multiplicity of infection (MOI) of 10, as

measured by flow cytometry for GFP expression in secondary cells, was less than 1%.

To inhibit lentiviral infection, 293 cells were infected with the viral supernatant in the presence or absence of 5 μM zidovudine (AZT; Sigma, St. Louis, MO).

To investigate the kinetics of LV vector production after HL vector infection, 4×10^5 Hep3B cells were infected with HL at various MOIs in six-well plates. The medium was collected at different time points and titrated on 293 cells, as described earlier.

Long-term culture experiments

Hep3B cells (2×10^5) were infected with the HL vector, at an MOI of 10, and incubated in the presence of AZT on a 10-cm dish. The cells were split at a ratio of 1:20 once a week, and expression of GFP was examined by flow cytometry. At each passage, DNA was extracted from a portion of the cells and analyzed for proviral integration by Southern hybridization. A part of the HL-infected cells were also plated on Lab-Tek chamber slides (Thermo Fisher Scientific, Rochester, NY). The next day, the cells were fixed for 10 min with 4% paraformaldehyde, washed with PBS, and incubated with 50 mM NH_4Cl in PBS for 5 min. The cells were permeabilized in 0.5% Triton/PBS for 5 min and then incubated for 30 min in 1% bovine serum albumin/PBS for blocking. The cells were incubated for 1 hr with a 1:1000 dilution of mouse anti-GFP monoclonal (Chemicon, Temecula, CA). Immunoreactivity for GFP was visualized with a 1:5000 dilution of goat anti-mouse immunoglobulin G (IgG) (H + L) Alexa Fluor 488. The cells were then incubated with a 1:1000 dilution of rabbit anti-βgal polyclonal (ab616; Abcam, Cambridge, MA). Immunoreactivities for βgal were visualized with a 1:5000 dilution of goat anti-rabbit IgG (H + L) Alexa Fluor 594 (Molecular Probes, Eugene, OR).

Animals

Chimeric mice with human liver were generated as previously described (Tateno *et al.*, 2004). Briefly, uPA/SCID mice were generated by crossing uPA mice [B6SJL-TgN(Alb1Plau)144Bri; The Jackson Laboratory, Bar Harbor, ME] with SCID mice (Fox Chase SCID C.B-17/Icr-*scid* Jcl; Clea Japan, Tokyo, Japan). The $uPA^{+/+}SCID^{+/+}$ mice were screened by polymerase chain reaction (PCR) and injected with $5.0–7.5\times10^5$ viable human hepatocytes (IVT079; In Vitro Technologies Inc., Baltimore, MD) through a small left-flank incision into the inferior splenic pole at 20–30 days after birth. The mice were injected intraperitoneally with 200 μl of 1.5 mg/ml Futhan (nafamostat mesilate, 6-amidino-2-naphthyl *p*-guanidinobenzoate dimethanesulfonate; gift from Torii Pharmaceutical, Tokyo, Japan) to enhance repopulation of the liver with human hepatocytes. The replacement index was estimated by serum level of human albumin as previously described (Tateno *et al.*, 2004). Generally, >5 mg/ml human albumin in the blood indicates high replacement index values of >70%, and mice screened in this manner were used for experiments at 6–8 weeks posttransplantation.

After injection with gadolinium (10 mg/kg body weight) to eliminate Kupffer cells (Lieber *et al.*, 1997), either HL vector (2×10^9 TU/200 ml) or buffer (PBS) was injected via tail vein, followed by sacrifice at 4 days or 4 weeks postinfection ($n = 4$ per group). A portion of each liver sample was immediately digested into cell suspensions and used for flow cytometric analysis. The remaining portion was frozen in liquid nitrogen for isolation of genomic DNA or for frozen tissue sections. Immunofluorescence (IF) and immunohistochemistry (IHC) for GFP were performed on frozen liver sections using standard methods with GFP-specific antibodies (ab290; Abcam): goat anti-rabbit IgG-Alexa Fluor 488 for IF, or Vectastain ABC kit (Vector Laboratories, Burlingame, CA) and diaminobenzidine for IHC. IF for βgal was also performed using rabbit anti-βgal antibodies (ab616; Abcam) and goat anti-rabbit IgG-Alexa Fluor 594, as earlier. X-gal staining using standard methods was also performed on glutaraldehyde-fixed liver sections, and the proportion of βgal-positive cells was determined by image analysis using the SPOT digital imaging system and NIH ImageJ software (version 1.34). The replacement index of the mouse liver with human hepatocytes was also determined by IHC for human-specific cytokeratin-8 and -18 (CK8/18) as previously described (Tateno *et al.*, 2004) and is defined as the ratio of area occupied by human hepatocytes to the entire area examined. To assess any potential hepatotoxicity, sera were collected from mice at the time of scheduled sacrifice, that is, at 4 weeks after injection with HL vector or PBS, and serum levels of aspartate amino transferase (AST) were measured by automated colorimetric assay.

Molecular analysis of integrated LVs in the liver

High-molecular-weight genomic DNA was extracted from livers injected with HL vector or PBS. For detection of the stably integrated form of the second-stage LV after production from the first-stage HDAdV, high-molecular-weight genomic DNA (500 ng) was subjected to nested PCR to amplify lentiviral integration events close to or within *Alu* repeat sequences in the human genome (Nguyen *et al.*, 2002; Serafini *et al.*, 2004). Briefly, the first PCR (PCR1) was carried out using a sense oligomer specific for the conserved sequences of human *Alu* (*Alu*-s; 5′-TCCCAGCTACTCGGGA GGCTGAGG-3′) and an antisense oligomer specific for the PBS region of HIV-1 upstream of *gag* (5NC2-as; 5′-GAGTC CTGCGTCGAGAGAG-3′). All amplifications were done using 100 μl of reaction mixture containing 200 ng of genomic DNA, 0.4 mM of each dNTP, 0.8 μM of each sense and antisense primer, 5% dimethyl sulfoxide, and 2 U *Taq* DNA polymerase. After the first DNA denaturation at 95°C for 5 min, 30 amplification cycles were performed consisting of denaturation for 1 min at 94°C, annealing for 1 min at 60°C, and extension for 3 min at 72°C. One aliquot (1:100 dilution) of the first PCR products was subjected to a second PCR (PCR2) amplification using the nested primers, LTR9-s (5′-GCCTCAATAAAGCTTGCCTTG-3′) and U5PBS-as (spanning the U5LTR/PBS boundary region) (5′-GGCGCCAC TGCTAGAGATTTT-3′), which amplified a fragment of 121 bp. The nested PCR conditions were similar to those of the first amplification, except for an annealing temperature of 55°C and an extension time of 1 min. Twenty amplification cycles were performed. In control reactions, genomic DNA that had not been subjected to the first round of PCR was also amplified using the second PCR primers to exclude the presence of residual nonintegrated vector DNA. As a loading control, the same DNA samples were subjected to a PCR that amplified a 610-bp region of human β-actin (5′-GATCAT GTTTGAGACCTTCA-3′ and the reverse sequence 5′-ACC

TTGATCTTCATGGTGC-3′), with the following amplification conditions: 95°C for 2 min, then 30 cycles of 95°C for 30 sec, 65°C for 30 sec, and 72°C for 1 min, followed by a final extension at 72°C for 5 min. Amplification products were resolved on 1.5% agarose gel containing ethidium bromide and detected by ultraviolet transillumination.

The copy number of the integrated form of the lentiviral construct in each cell was determined by quantitative real-time PCR (Q-PCR) with βgal-specific primers and probe, designed using Primer Express software V. 1.0 (Applied Biosystems, Foster City, CA). Primer and probe sequences spanned a 91-bp region in the βgal-coding region, consisting of the following sequences: forward primer, 5′-CTATCCC GACCGCCTTACTG-3′; reverse primer, 5′-GTTTTCGCTCG GGAAGACGTA-3′; probe, 5′-FAM-CAGCGGTCAAAA CAG-TAMRA-3′. Amplification was performed in a reaction volume of 25 μl under the following conditions: 300 ng of high-molecular-weight genomic DNA, 1×Taqman universal PCR master mix (Applied Biosystems), 600 n*M* forward primer, 900 n*M* reverse primer, and 100 n*M* probe. Thermal cycling conditions were 2 min incubation at 50°C, 10 min at 95°C, followed by 40 cycles of successive incubation at 95°C for 15 sec and 60°C for 1 min. Standard curves were generated using serial dilutions of HL vector plasmid, pHL, from 5 to 50,000,000 copies in a background of 50,000 equivalents (300 ng) of untransduced genomic DNA from the chimeric mouse liver. Duplicate samples were amplified in an ABI Prism 7700 sequence detector with continuous fluorescence monitoring. Data were collected and analyzed using 7700 Sequence Detection System software v.1.6.3. (Applied Biosystems). The copy number per cell of integrated lentiviral construct was calculated as the average copy number divided by 50,000 cells (equivalent to 300 ng genomic DNA).

Statistical analysis

The results are presented as mean ± standard deviation. Statistical significance of differences was calculated using Student's *t*-test, and a *p*-value of <0.01 was considered significant.

Results

Design and production of the HL hybrid vector

The hybrid vector HL contains a complete set of HIV-derived lentiviral packaging components incorporated into an HDAdV (Fig. 1A), including (1) a multiple attenuated packaging construct expressing *gag-pol*, *rev*, and the *rev* response element sequence, (2) an envelope construct expressing amphotropic (i.e., broad mammalian host range) *env* from MLV strain 4070A, and (3) a minimal HIV-based LV transfer vector encoding a βgal marker gene driven by a methylation-resistant MLV promoter (MND promoter) (Chen *et al.*, 2002). As this transfer vector sequence contains a LV packaging signal so that its mRNA will be encapsidated by the coexpressed packaging and envelope components to form LV virions, the βgal transgene will not only be expressed in cells directly infected by the HDAdV, but also be transmitted to adjacent cells. The adenoviral backbone

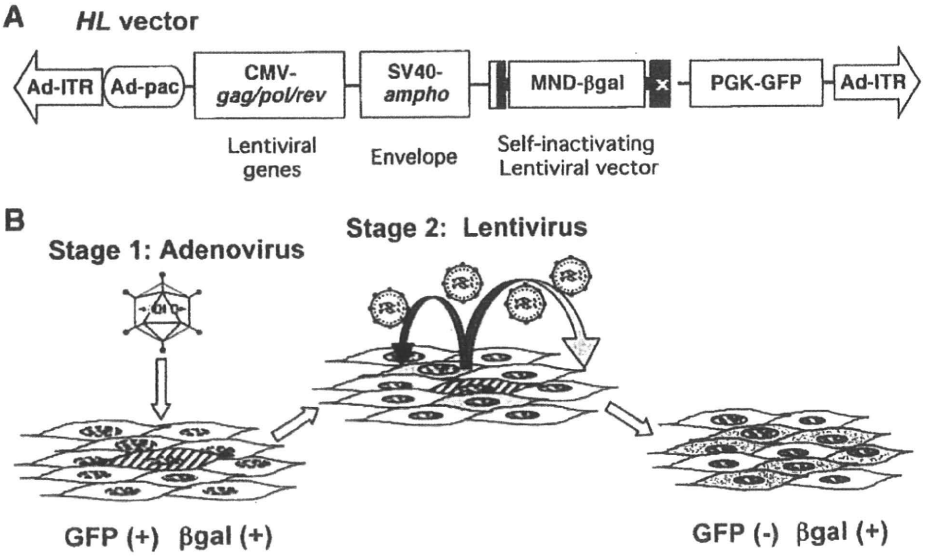

FIG. 1. Outline of the high-capacity adenovirus/lentivirus hybrid vector (HL vector) system. (**A**) Schematic structure of the HL vector. An HL vector is a helper-dependent adenoviral vector encoding expression cassettes for production of a lentiviral vector (LV) based on human immunodeficiency virus 1 (HIV-1). The HL vector has two inverted terminal repeats (Ad-ITR) and the packaging signal (Ad-pac) of human adenovirus type 5 and encodes four gene expression cassettes: (1) a self-inactivating minimal LV that contains the central polypurine tract, the woodchuck hepatitis virus posttranscriptional regulatory element, and the β-galactosidase gene (βgal) driven by the methylation-resistant murine leukemia virus LTR promoter (MND) (Robbins *et al.*, 1998; Chen *et al.*, 2002) as a marker; (2) HIV-*gag/pol/rev* coding sequences driven by cytomegalovirus (CMV) promoter; (3) the amphotropic murine leukemia virus envelope driven by the simian virus 40 early promoter (SV40) for pseudotyping of the lentivirus; and (4) the enhanced green fluorescent protein (GFP) driven by phosphoglycerokinase (PGK) promoter as a marker of the adenoviral backbone. (**B**) Two-stage transduction with the HL vector. The HL vector infects the initial target cells efficiently as an adenoviral vector and produces an LV *in situ*. The LV then infects surrounding secondary target cells and integrates into chromosomes for stable gene expression.

sequence also contains a GFP expression cassette unlinked to the LV components; the GFP marker gene will not be encapsidated into LV particles, thereby allowing specific quantitation of initial transduction by HDAdV itself. Thus, it is possible to distinguish between untransduced cells [GFP (−), βgal(−)], cells transduced by HL first-stage HDAdV only [GFP(+), βgal(+)], and cells transduced by HL second-stage LV [GFP(−), βgal(+)] (Fig. 1B).

The first-stage HDAdV was propagated using the FRT/FLPe helper system (Umana *et al.*, 2001). The GFP titers of purified HL vector preparations on 293 cells ranged from 4.1×10^9 to 1.8×10^{10} TU/ml. Vector stocks contained less than 0.1% helper virus contamination, as determined by Southern hybridization, using a probe for the adenoviral packaging signal (data not shown).

Infection with HL first-stage HDAdV results in production of functional second-stage LV

Following infection by the HL first-stage HDAdV vector at various MOIs, cell-free conditioned media from various human cell lines, including Gli36 (glioma), HeLa (cervical adenocarcinoma), and Hep3B and HepG2 (both hepatocellular carcinoma), were inoculated into fresh 293 cell cultures and tested for their ability to mediate secondary transmission of βgal expression. For all primary target cell lines tested, increasing MOI during first-stage HDAdV transduction correlated with increasing βgal transmission to secondary target cells (Fig. 2A). Further, βgal expression in secondary target cells was markedly suppressed by the reverse transcriptase inhibitor AZT, indicating that the observed transmission was indeed mediated by second-stage LV and was not due to carry-over of the first-stage HDAdV or pseudotransduction by overexpressed βgal protein (Fig. 2B). Of the cell lines tested, Gli36 and Hep3B produced the highest titers of LV (1.0×10^4 and 5.1×10^4 TU/ml, respectively, at MOI = 100) (Fig. 2A), which also correlated with high levels of p24 production (236 and 316 ng/ml, respectively). Primary human hepatocytes also produced LV at titers of 6.0×10^1, 1.0×10^3, and 1.2×10^4 TU/ml upon infection with 1, 10, and 100 μl of HL vector (4.0×10^8 TU/ml), respectively. Taken together, these findings indicate that the HL hybrid vector is

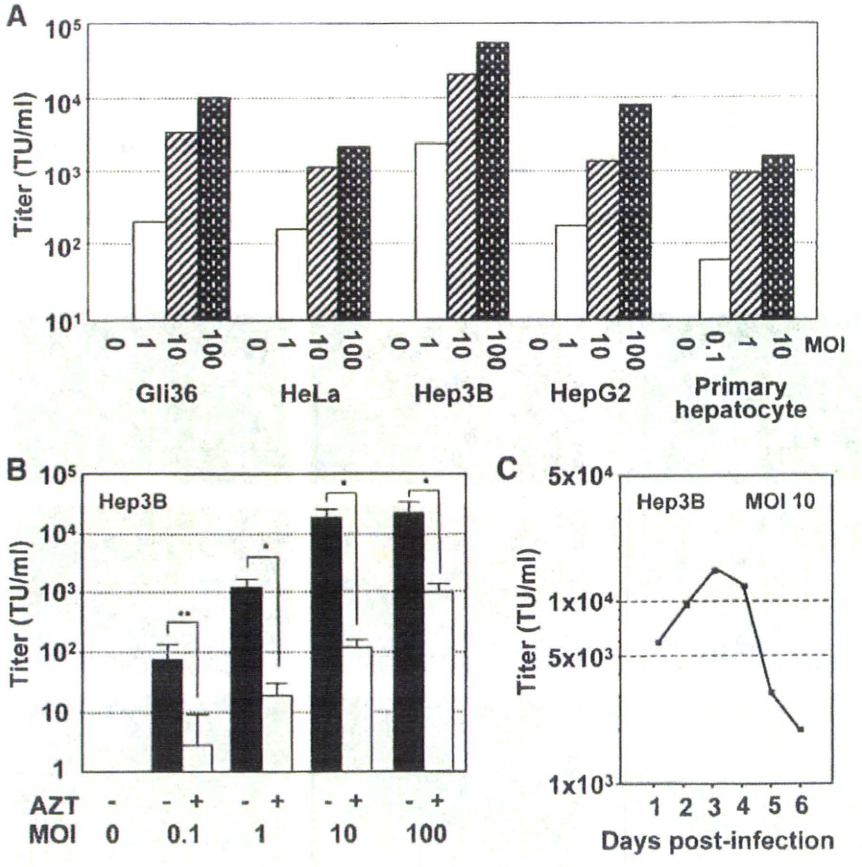

FIG. 2. Production of LV via HL vector system. (A) Production of LV in a variety of cell types after HL infection. Various cell lines indicated in the figure were infected with HL at multiplicity of infections (MOIs) of 1, 10, or 100. After 48 hr, viral supernatant was collected and titrated on 293 cells for βgal expression. (B) Production of LV following HL vector infection. Hep3B cells were infected with the HL vector at MOIs of 0.1, 1, 10, or 100. After 48 hr, viral supernatant was collected and titrated on 293 cells for βgal expression in the presence or absence of zidovudine (AZT, 5 μM). Data shown are average titers and standard deviations from the experiment performed in triplicate. Effect of AZT on titers was determined by Student's *t*-test (**$p < 0.05$, *$p < 0.01$). (C) Time course of lentiviral production from Hep3B cells infected with the HL vector. Hep3B cells were infected with HL at an MOI of 10 and monitored for up to 6 days. At different time points indicated in the figure, the medium was replaced, and the viral supernatant was titrated for βgal expression on 293 cells.

capable of directing the production of infectious LV particles from a variety of cell types, and that the LV yield is dependent upon the MOI and the target cell type.

To determine how long cells can produce LV after being infected with the HL first-stage HDAdV vector, a time-course experiment was performed. After infection of Hep3B cells with the HL first-stage HDAdV vector at an MOI of 10, the culture medium was harvested and replaced with fresh medium every day. The LV titers of the conditioned media harvested daily were measured on secondary target cells and were found to increase, reaching a peak level by day 3 post-HDAdV infection (1.3×10^4 TU/ml; Fig. 2C). Thereafter, HL-infected human cells continued to sustain LV production for several days (postinfection day 6 titer = 2.0×10^3 TU/ml).

In vitro *persistence of second-stage LV-transduced cells following HL first-stage HDAdV infection*

The spread of lentivirus in long-term cultures of HL-infected cells was examined by maintaining infected Hep3B in culture (Fig. 3A). As expected, GFP expression from the adenovirus backbone significantly decreased over time because of ongoing cell division-mediated dilution of HDAdV episomes in the culture. The percentage of GFP-positive cells

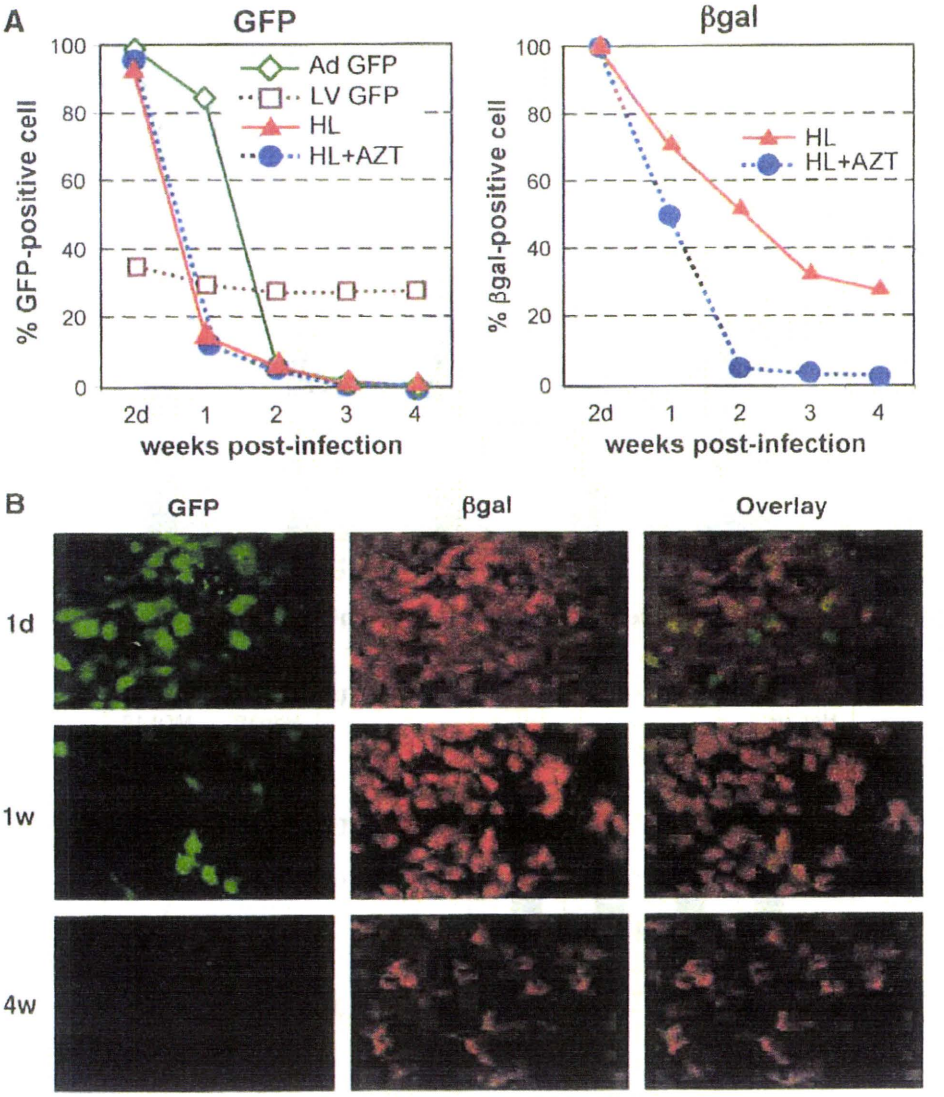

FIG. 3. Spread of LV-transduced cells and persistent gene expression following HL vector infection. (A) Transduction efficiencies of HL hybrid vector-infected cells. Hep3B cells (2×10^5) infected with the HL vector at an MOI of 10 were incubated overnight, and the cells were split the following day and cultivated in the presence (blue circle) or absence (red triangle) of AZT on a 10-cm dish. The control samples infected with an LV GFP (brown square) or an Ad GFP (green diamond) are also shown. The cells were passaged at a ratio of 1:20 every week, and expressions of GFP and βgal were examined. Data are representative of three independent experiments, all yielding similar results. (B) Persistent gene expression achieved via HL hybrid vector system in transformed human hepatocytes *in vitro*. Hep3B cells were infected with HL vector at an MOI of 10. The cells were passaged at a ratio of 1:20 every week. Expressions of GFP and βgal were analyzed by immunofluorescence staining using anti-GFP and anti-βgal antibody at the indicated time points after HL infection.

quickly decreased from >90% to <2% within 2 weeks postinfection in the HL-infected cells (HL and HL + AZT) as well as in cells infected with control Ad GFP. Initially, a parallel decrease in βgal-positive cells was observed. However, 25% of the HL-infected cells (HL) remained βgal positive at 4 weeks postinfection, whereas those in the HL-infected/AZT-treated cells (HL + AZT) were <2% βgal positive within 2 weeks postinfection. Persistent βgal expression in the HL-infected cells (HL) was also confirmed by IF staining (Fig. 3B). Southern hybridization of high-molecular-weight genomic DNA extracted from the cells at week 4 confirmed LV proviral integration and a direct correlation between βgal expression and the copy number of the integrated βgal transgenes (data not shown). This also demonstrates that persistent βgal expression in the HL-infected cells is mediated by stable transduction with the HL second-stage LV vector.

In vivo *persistence of second-stage LV-transduced cells in humanized liver following intravenous administration of HL first-stage HDAdV*

In vivo testing of the HL vector system requires a model that is permissive for assembly of human lentivirus. We employed a unique humanized model in which endogenous murine hepatocytes are extensively replaced with human hepatocytes. The replacement indices, calculated as the frequency of human-specific CK8/18-positive regions relative to that of the entire examined area in the mouse liver (Tateno *et al.*, 2004), ranged from 63.7% to 86.6% (Fig. 4A). This model was found to be efficiently transduced by control HDAdV (HDΔ28E4LacZ) (Palmer and Ng, 2003) (data not shown), and so chimeric uPA/SCID mice with highly humanized livers were intravenously injected with the HL first-stage HDAdV vector.

First, GFP expression from the adenoviral backbone of the HL first-stage HDAdV in liver tissue was analyzed by flow cytometry. The results showed 7.64% ± 1.33% GFP-positive cells at 4 days postinfection and 0.21% ± 0.07% GFP-positive cells at 4 weeks postinfection. This reduction in GFP-positive hepatocytes was also confirmed by IF (Fig. 4B) and IHC (Fig. 4C).

On the other hand, βgal expression persisted for at least 4 weeks postinfection as shown by IF studies (Fig. 4D) and X-gal tissue staining (Fig. 4E). Quantitation by image analysis revealed that the percentage of βgal-positive cells increased from 16.21% ± 3.70% at 4 days, to 28.40 + 4.92% at 4 weeks postinfection ($p = 0.0074$). The persistence of βgal expression suggested that stable integration by the second-stage LV might have occurred. To demonstrate integration of second-stage LV in human hepatocyte genomic DNA *in vivo*, nested *Alu*–lentivirus PCR was performed (Nguyen *et al.*, 2002; Serafini *et al.*, 2004). In this assay, the first round of PCR was performed using a sense primer specific for human *Alu* sequences and another primer specific for the lentiviral 5′ noncoding region as the antisense primer (*Alu*-s and 5NC2-as, respectively; Fig. 5A). As LV vectors randomly integrate at multiple sites and repetitive *Alu* sequences are scattered throughout the human genome, the first reaction generated products with variable sizes (Fig. 5B, PCR1). The second round of PCR, using nested primers within the viral LTR and the viral primer binding site, respectively ("LTR9-s" sense and "U5 PBS-as" antisense primers, as depicted in Fig. 5A), generated the expected 140-bp product from transduced liver tissues, but not from untransduced control liver (Fig. 5B, PCR1 + PCR2). Genomic DNA from transduced cells subjected only to second-round PCR amplification did not yield any signal, validating the inability of the nested primers alone to amplify any residual episomal LV sequences and confirming the requirement for first-round amplification with the *Alu*–lentivirus primers to detect integrated proviruses (Fig. 5B, PCR2). Although this is not a quantitative assay, taken together these results do demonstrate integration of the lentiviral sequences into the genome of human hepatocytes *in vivo*.

For further quantitative assessment of the percentage of cells expressing βgal from the lentivirus vector component, Q-PCR was again performed, this time using high-molecular-weight genomic DNA from each of liver tissues as the template and with primers and probe specific for the βgal gene. The Q-PCR results demonstrated that the percentage of βgal-positive cells was 13.8–56.6% at 4 weeks postinfection, correlating with the data obtained by Xgal staining (28.40% ± 4.92%) (Fig. 4E). These results indicate that *in situ* production and spread of second-stage LV had occurred in the humanized livers of chimeric mice following systemic administration of the HL first-stage HDAdV, and taken together with the above finding that the first-stage HDAdV was undetectable at 4 weeks postinfection, it is likely that βgal expression at a later time point is derived almost entirely from the second-stage LV.

To assess any potential vector-related hepatotoxicity, serum AST levels were measured and compared between HL vector-injected and control PBS-injected mice. It should be noted that the levels of serum liver enzymes in the uPA/SICD-based chimeric mouse model are generally high because of the ongoing hepatic expression of uPA, which mediates progressive destruction of murine hepatocytes and thereby allows gradual engraftment of human hepatocytes. Notably, however, there was no significant difference in the serum AST levels between HL-injected mice (272.5 ± 154.5 U/l) and PBS-treated group (453.0 ± 79.3 U/l) ($p = 0.1546$). Consistent with these findings, liver histology showed no significant difference between PBS- and HL vector-treated livers. Taken together with the serum AST levels, this indicates that the HL vector does not cause significant liver toxicity. In addition, as noted earlier, serum levels of human albumin remained at high values (>5 mg/ml) throughout these experiments, and replacement indices remained at high levels, ranging from 63.7% to 86.6% (Fig. 4A), further indicating that the HL vector does not show any selective toxicity that would alter the proportion of human hepatocytes.

Discussion

The liver has a variety of characteristics that make it a significant target for gene therapy (Ferry and Heard, 1998). As the liver is the site of essential metabolic pathways, it is involved in many inborn metabolic diseases. Moreover, because of its highly vascularized architecture and position as a portal to blood circulation, the liver can serve as a secretory organ for the systemic delivery of therapeutic proteins. Because of the fenestrated structure of its endothelium, the liver parenchyma is readily accessible to large molecules such as DNA or recombinant viruses via the blood stream. AdVs accumulate